

Regression coefficient estimation from remote sensing maps

Kerri Lu^{*1,2}, Dan M. Kluger^{*4}, Stephen Bates^{*1,2}, and Sherrie Wang^{*1,3,4}

¹Laboratory for Information and Decision Systems, MIT

²Department of Electrical Engineering and Computer Science, MIT

³Department of Mechanical Engineering, MIT

⁴Institute for Data, Systems, and Society, MIT

Abstract

Remote sensing map products are used to estimate regression coefficients relating environmental variables, such as the effect of conservation zones on deforestation. However, the quality of map products varies, and — because maps are outputs of complex machine learning algorithms that take in a variety of remotely sensed variables as inputs — errors are difficult to characterize. Thus, population-level estimates from such maps may be biased. In this paper, we apply prediction-powered inference (PPI) to regression coefficient estimation. PPI generates unbiased estimates by using a small amount of randomly sampled ground truth data to correct for bias in large-scale remote sensing map products. Applying PPI across multiple remote sensing use cases in regression coefficient estimation, we find that it results in estimates that are (1) more reliable than using the map product as if it were 100% accurate and (2) have lower uncertainty than using only the ground truth and ignoring the map product. Empirically, we observe effective sample size increases of up to 17-fold using PPI compared to only using ground truth data. This is the first work to estimate remote sensing regression coefficients without assumptions on the structure of map product errors. Data and code are available at <https://github.com/Earth-Intelligence-Lab/uncertainty-quantification>.

1 Introduction

Remote sensing maps are widely used to obtain estimates for environmental quantities, such as cropland expansion over time or the effect of protected areas on deforestation (Baccini et al., 2012; Deines et al., 2019; Hansen et al., 2013; Potapov et al., 2022; Wang et al., 2019). Map products created by training machine learning models on remotely sensed data allow researchers to cheaply access predictions for a variable of interest at a high resolution over large regions.

However, the quality of map products varies, and resulting population-level estimates of quantities of interest may be biased (Bastin et al., 2017; Jain, 2020; Venter et al., 2024). For example, Bastin et al. (2017) showed that human labeling of high-resolution imagery results in an estimate of global forest extent in dryland biomes that is 40% to 47% higher than previous estimates from remotely sensed forest cover map products. Moreover, different map products may conflict with each other and result in significantly different estimates over the same region. For example, Alix-Garcia and Millimet (2023) found that two commonly used satellite-based remote sensing maps of forest cover in Mexico differ significantly from each other, implying that there is misclassification error in at least one of the algorithms used to categorize pixels as forest or non-forest. Another recent study (Venter et al., 2022) of three satellite-based global land cover/land use map products found that the maps are biased toward different land cover classes (e.g., one map overestimates shrub cover and another overestimates grass cover relative to the other maps).

Errors in map products are often difficult to characterize due to the complexity of input data and lack of interpretability in the ML models used to generate the maps. Examples of systematic errors in map products trained on satellite data include “nonrandom misclassification, saturation effects, atmospheric effects, and

*Email: {kerrilu, dkluger, stephenbates, sherawang}@mit.edu

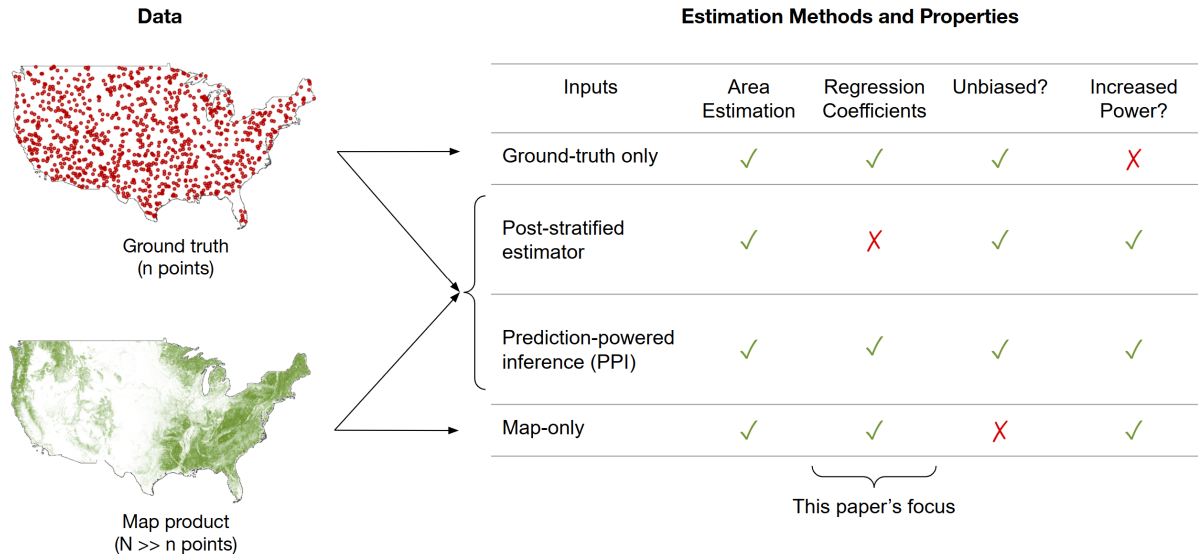


Figure 1: **Overview of estimation methods using ground truth data and remote sensing map products.** The post-stratified estimator (for area estimation) and prediction-powered inference (for regression coefficient estimation) use a small amount of ground truth data along with a map product to produce confidence intervals for the quantity of interest. In this paper, we focus on regression coefficient estimation using PPI. We also compare PPI against GT-only (using only ground truth) and map-only estimators.

cloud cover,” all of which may lead to biased inference (Jain, 2020). This has prevented environmental scientists, economists, and policymakers from using remote sensing maps in their analyses. The World Bank Group (2018) has cited uncertainty in remote sensing maps as a barrier to their use in water resources management, and the United Nations Satellite Imagery and Geospatial Data Task Team (2017) wrote that the “shift in paradigm from traditional statistical methods (e.g., counting, measuring by humans) towards estimation from sensors (with associated aspects of validity, approximation, uncertainty)... will require convincing, statistically sound results.” Correctly accounting for map errors, then, is crucial for maximizing the potential of remote sensing data to expand scientific knowledge and advance practical operations.

For those who currently reject estimation from remote sensing as too unreliable, the alternative is to use ground truth observations for the variable of interest. However, ground truth data is often sparse because it is expensive to collect, as it may require fieldwork or manual labelling of remote sensing imagery. Few ground truth points result in greater uncertainty (i.e., wider confidence intervals) in estimates.

Another alternative is to use both ground truth data and remote sensing maps to generate estimates, using the ground truth points to correct for biases that may exist in the map products. This generally reduces uncertainty in the estimates compared to using ground truth alone, since map products contain a large amount of data that, while possibly biased, still give useful information about the true values we wish to measure.

As an example of this approach, the remote sensing community commonly uses a **post-stratified estimator** to generate confidence intervals for **area estimation**. A **pixel-counting estimator**, which uses only a map product to estimate area of a land cover class, may be biased due to misclassification error in the map product (Olofsson et al., 2020). An unbiased area estimate can be obtained by using randomly sampled ground truth data (Olofsson et al., 2014; Stehman and Foody, 2019), but if ground truth observations are sparse, this may result in less precise estimates (wider confidence intervals) than desired. To resolve this, the post-stratified area estimator (Card, 1982; Olofsson et al., 2013; Stehman, 2013) combines a map product with a small amount of ground truth data, using the confusion matrix between land cover ground truth and map product points to correct for bias in the map product. By leveraging the map product, the post-stratified estimator also produces narrower confidence intervals compared to only using ground truth data. Other area estimators that combine ground truth and map product data, including regression, ratio, and calibration estimators, are described in Gallego (2004).

Coefficient estimates

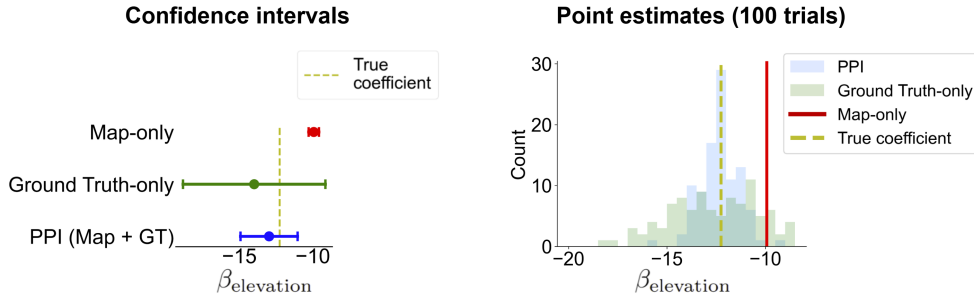


Figure 2: **Motivating example: PPI produces unbiased coefficient estimate with lower variance than using ground truth alone.** We estimate the linear regression coefficient relating US forest cover to elevation (with $N = 67968$ remote sensing map points and $n = 500$ ground truth points). Left: Map-only, ground truth-only, and PPI point estimates and 95% confidence intervals. Right: Histogram of PPI and GT-only point estimates from repeating the experiment with 100 random sets of $n = 500$ ground truth points.

The remote sensing community also uses map products for **regression coefficient estimation**: estimating linear or logistic regression coefficients for causal or associative relationships between two or more environmental variables. Unlike area estimation with the post-stratified estimator, regression coefficient estimation from remote sensing maps still suffers from bias due to map product errors. An unbiased estimate can be obtained by running a regression on randomly sampled ground truth data (Särndal et al., 2003), but similarly to the area estimation case, this may result in less precise estimates than desired.

In this paper, we address this problem by applying **prediction-powered inference (PPI)** to regression coefficient estimation (Figure 1). PPI (Angelopoulos et al., 2023a,b; Kluger et al., 2025) is a recently developed unbiased estimation method that uses a small set of randomly sampled ground truth observations (n points) to calibrate and correct for bias in a much larger set of machine learning-generated predictions (N points, where N is much larger than n). This method also results in more precise estimates (higher statistical power, smaller confidence intervals) than using the ground truth points alone. We apply PPI to regression use cases where the machine learning predictions are obtained from large-scale remote sensing map products. We compare results with the **ground truth-only (GT-only) estimator** (using only ground truth points) and **map-only estimator** (using only a map product). These estimators are described in detail in Section 2.

A motivating example. We give a brief preview of how we use PPI to correct map products with ground-truth data to obtain an unbiased regression coefficient estimate.

We seek to estimate linear regression coefficients for the association between US forest cover and a few covariates, including elevation. We use $N = 67968$ remote sensing map product points and $n = 500$ ground truth points. See Section 3.1 for a complete description of the experimental setup.

We compare the 95% confidence intervals for the elevation coefficient estimates from PPI, GT-only, and map-only methods (Figure 2, left panel). The “GT-only” estimate using only ground truth points is unbiased but has the widest confidence interval, failing to take advantage of existing map products. Meanwhile, PPI uses the map product along with the ground truth points to produce a much smaller confidence interval while still being unbiased. The PPI and GT-only confidence intervals both contain the true coefficient, while the confidence interval estimated from the map product alone does not. That is, if we had used only the map product, we would have underestimated the magnitude of the negative relationship between forest cover and elevation. PPI avoids misleading conclusions by using ground truth points to correct for bias, and at the same time, it gives smaller confidence intervals than using only the ground truth points.

We repeat the experiment using the same set of $N = 67968$ map product points and 100 different randomly chosen sets of $n = 500$ ground truth points (see Appendix C.4 for more detail). A histogram of the 100 PPI and GT-only elevation coefficient point estimates is shown in the right panel of Figure 2. As

Regression type	Response variable	Covariates	Region	Year	Map product(s)	Ground truth	Link to code
Logistic	Deforestation	Distance from roads, distance from rivers, elevation, slope	Brazilian Amazon	2000-2015	NASA Global Forest Cover Change (Townshend, 2016)	$n = 1386$ from (Bullock et al., 2020)	link
Linear	Tree cover	Aridity index, elevation, slope	Contiguous USA	2021	USFS Tree Cover (USDA Forest Service, 2023)	$n = 983$ manually labeled images (Sec. 3.1)	link
Linear	Housing price	Income, nightlights, road length	Contiguous USA	2010-2021	MOSAICS (Rolf et al., 2021)	$n = 500$ from (Rolf et al., 2021)	link
Linear	Forest cover	Elevation, population	Contiguous USA	2010	MOSAICS (Rolf et al., 2021)	$n = 500$ from (Rolf et al., 2021)	link

Table 1: **Overview of use cases and datasets.** To illustrate the mechanics and advantages of PPI, we estimate linear regression coefficients for tree cover, housing price, and forest cover in the United States. Code implementations of the use cases are linked in the rightmost column.

before, we see that the PPI and GT-only estimators are both unbiased relative to the true coefficient, but the PPI estimates are more precise as they have a lower variance than the GT-only estimates.

Our contribution. In this paper, we illustrate the use of PPI on four specific regression coefficient estimation tasks associating deforestation, tree cover, housing price, and forest cover to other geospatial variables; see Table 1. We then simulate map error to understand its influence on the bias and variance of map-only, GT-only, and PPI estimators. We demonstrate that PPI can be applied when there is error in the remotely sensed response variable, the remotely sensed covariates, or both. Data and code for these use cases are available at <https://github.com/Earth-Intelligence-Lab/uncertainty-quantification>.

Using PPI to combine ground truth data with map products results in unbiased estimates that are more reliable than map-only estimates and have lower uncertainty than GT-only estimates. As we will show, map-only estimators without bias correction can result in incorrect regression coefficient estimates.

To improve the utility of machine learning-generated remote sensing maps for downstream regression applications, we recommend that map *producers* provide a randomly sampled holdout ground truth dataset to be used for calibration in PPI alongside their maps, or, if that is not done, for map *users* to generate their own randomly sampled holdout set for calibration, if possible (e.g., from visual inspection of remote sensing data). This holdout set can be obtained by simple (uniform) random sampling or other sampling designs such as stratified, weighted, or clustered random sampling (Kluger et al., 2025).

Related work. Previous works have developed methods to reduce bias in regression coefficient estimates from remote sensing data. For example, Alix-Garcia and Millimet (2023) estimates the effect of a conservation program on deforestation in Mexico. They correct for bias in the remotely sensed deforestation binary variable by modelling misclassification probabilities as a parametric function of environmental covariates. However, this approach imposes assumptions about the structure of the misclassification errors and moreover is only developed for settings with binary response variables. Another study (Gordon et al., 2023) estimates logistic regression coefficients for the relationship between roads and forest cover in West Africa. They train an adversarial debiasing model with ground truth data to correct for bias arising from correlations between distance from roads and the measurement error in remotely sensed forest cover; however, they do not provide an approach for constructing confidence intervals. Another study (Proctor et al., 2023) uses co-located ground truth and remotely sensed data to show that using remote sensing data alone leads to biased regression coefficient estimates for several effect size estimation tasks in the US. To remedy this issue, they propose using a Bayesian linear measurement error model and applying multiple imputation: a statistical method that involves estimating the missing values in a dataset and their uncertainties and fitting the regression on multiple randomly imputed versions of the dataset. Note that this method requires an assumption about the error structure of the remotely-sensed variables and does not have any frequentist coverage guarantees. For example, in a subset of the simulation-based experiments in Proctor et al. (2023), 95% confidence intervals from multiple imputation only contained the true value of the regression coefficient

in fewer than 80% of the simulations as opposed to the desired $\sim 95\%$ of the simulations. In contrast to existing approaches in the remote sensing literature, PPI does not make any modelling assumptions about the measurement error structure, and under certain regularity conditions, its confidence intervals are guaranteed to attain the desired coverage (Angelopoulos et al., 2023a,b; Kluger et al., 2025).

Another approach to uncertainty quantification is *conformal prediction* (Angelopoulos and Bates, 2023; Vovk et al., 2005), which generates confidence sets for machine learning predictions at individual data points. For example, Valle et al. (2023) applies conformal prediction to quantify pixel-level uncertainty for a land cover/land use map product in the Brazilian Amazon, outputting a 90% predictive set of land cover classes for each pixel (i.e., the set contains the true land cover class 90% of the time). This approach differs from our work because PPI estimates regression coefficients over an entire region, rather than quantifying uncertainty of map estimates at individual points or pixels.

Unlike previous works, this paper is the first work to apply prediction-powered inference to remote sensing use cases in regression coefficient estimation. This is also the first work to combine map product and ground truth data to estimate remote sensing regression coefficients without assuming an error structure on the map product predictions.

2 Methods: Prediction-Powered Inference for Regression

Regressions are commonly used in the environmental sciences and economics to identify relationships — associative or causal — between covariates and a binary response (logistic regression) or between covariates and a continuous response (linear regression). Logistic regression coefficients give the change in the log-odds ratio of a binary response corresponding to a one-unit increase in a covariate, when all other covariates are held constant. Linear regression coefficients give the change in the value of a continuous response corresponding to a one-unit increase in a covariate, when all other covariates are held constant. Thus, we can interpret these coefficients as effect sizes of the covariates.

Historically, scientists would run regressions using ground truth environmental samples, but regressions on data from remote sensing maps are becoming increasingly common, e.g., (Deines et al., 2019, 2023; He et al., 2022; Lobell et al., 2022; Taylor and Druckenmiller, 2022; Taylor and Heal, 2023). When covariate or response variable values are machine learning predictions from a map product, errors in the machine learning model may result in biased regression coefficients (as we have seen in Figure 2).

In this section, we formally describe how to use **prediction-powered inference (PPI)** to generate regression coefficient estimates and confidence intervals when the response variable Y and/or covariates X are remotely sensed map products. As two baselines, we consider the **ground truth-only estimator** that only uses ground-truth data (which is unbiased but does not leverage remote sensing maps) and the **map-only estimator** that only uses remote sensing maps (which may be biased). We then describe PPI, which uses both sources of data to produce unbiased confidence intervals. Figure 1 summarizes the methods. As a technical note, this paper focuses on inference in settings where both the ground truth data and the larger sample from a remote sensing map product are assumed to be randomly sampled from a superpopulation, as opposed to a design-based inference framework for reasons discussed in Appendix A.

Suppose we have a remote sensing data product with a large number N of predictions $(\hat{X}'_1, \hat{Y}'_1), (\hat{X}'_2, \hat{Y}'_2), \dots, (\hat{X}'_N, \hat{Y}'_N)$ where $X \in \mathbb{R}^p$ is a vector of covariates and $Y \in \mathbb{R}$ is the response variable. Suppose that for a small **calibration set** of $n \ll N$ points sampled uniformly at random, we have ground truth labels $(X_1, Y_1), (X_2, Y_2), \dots, (X_n, Y_n)$ with corresponding remote sensing predictions $(\hat{X}_1, \hat{Y}_1), (\hat{X}_2, \hat{Y}_2), \dots, (\hat{X}_n, \hat{Y}_n)$. (Note that in some use cases, ground truth data may be widely available either for the response variable, for a subset of the covariates, or for a subset of both. In these cases, we would use ground truth instead of remotely sensed values for the corresponding components of the (\hat{X}, \hat{Y}) and (\hat{X}', \hat{Y}') vectors.)

2.1 Linear regression

In the case of linear regression, we wish to estimate 95% confidence intervals for the regression coefficients β_* giving the best fit to the linear model

$$Y = \beta^T X + \epsilon,$$

where ε is mean 0 and uncorrelated with X . (We assume that the first element of the vector X is a constant 1, so that the first regression coefficient β_0 is an intercept term.)

Ground truth-only estimator. The ground truth-only (GT-only) estimator uses only the n ground truth calibration datapoints to compute the regression coefficient estimate

$$\hat{\beta}_{\text{calib}} = \arg \min_{\beta} \sum_{i=1}^n (Y_i - \beta^T X_i)^2.$$

However, the standard error of this ground truth coefficient estimate will be large when the number of ground truth observations n is small, which is often the case in environmental applications. As a result, the GT-only 95% confidence interval will be large.

Map-only estimator: Use only the remote sensing map. The map-only estimator uses only the N map data points to compute the regression coefficient estimate

$$\hat{\gamma}_{\text{map}} = \arg \min_{\beta} \sum_{i=1}^N (\hat{Y}_i' - \beta^T \hat{X}_i')^2.$$

The standard error of the map-only coefficient estimate will be small if N is large, resulting in a small map-only 95% confidence interval. However, we employ the γ notation to emphasize that the map-only estimator may be *biased*; if the remotely sensed values \hat{X}_i' or \hat{Y}_i' are inaccurate, $\hat{\gamma}_{\text{map}}$ might be biased in the sense that as the sample size goes to infinity, $\hat{\gamma}_{\text{map}}$ will converge (in probability) to some $\gamma_* \neq \beta_*$. Thus, the map-only confidence interval is not guaranteed to have the appropriate coverage rate (in this case, 95%) of the true parameter of interest. This is because the map-only estimator does not account for error or uncertainty in the model used to generate the map product predictions.

Prediction-Powered Inference: Map + ground truth. Introduced in 2023, **Prediction-Powered Inference (PPI)** (Angelopoulos et al., 2023b) is an uncertainty quantification approach that computes confidence intervals using a small calibration set of ground truth points and a much larger set of machine learning-generated predictions. The main idea is that PPI assesses the bias in the map product using the ground truth data and then corrects it. For regression coefficient estimation, we use variants of PPI that were developed in Kluger et al. (2025) and have origins in Y.-H. Chen and H. Chen (2000) and Zrnic (2024). (PPI can also be applied to mean and area estimation; see Appendices D and E.)

PPI uses the calibration data to correct for bias in the map-based estimate. First, it computes the regression coefficient estimate using the remote sensing predictions at the n calibration datapoints:

$$\hat{\gamma}_{\text{calib}} = \arg \min_{\beta} \sum_{i=1}^n (\hat{Y}_i - \beta^T \hat{X}_i)^2.$$

Then, the PPI regression coefficient estimate corrects the map-only estimate $\hat{\gamma}_{\text{map}}$ for bias, using the difference between the ground truth and map estimates on the calibration set ($\hat{\beta}_{\text{calib}} - \hat{\gamma}_{\text{calib}}$). The final PPI estimate is

$$\hat{\beta}_{\text{PPI}} = \underbrace{\hat{\gamma}_{\text{map}}}_{\text{map-only estimate}} + \underbrace{(\hat{\beta}_{\text{calib}} - \hat{\gamma}_{\text{calib}})}_{\text{bias correction}}.$$

The PPI estimate can be improved by computing a tuning matrix $\hat{\Omega}$ that minimizes the variance of each component of the estimated coefficient vector. The value of $\hat{\Omega}$ depends on the quality of the map product relative to the ground truth. The tuned PPI regression coefficient estimate is

$$\hat{\beta}_{\text{PPI}} = \underbrace{\hat{\Omega} \hat{\gamma}_{\text{map}}}_{\text{map-only estimate}} + \underbrace{(\hat{\beta}_{\text{calib}} - \hat{\Omega} \hat{\gamma}_{\text{calib}})}_{\text{bias correction}}. \quad (1)$$

The tuned $\hat{\beta}_{\text{PPI}}$ is still an unbiased estimate for the true coefficient β_* . The analytic formula for an optimal choice of tuning matrix is presented in Appendix B for interested readers.

We compute a PPI confidence interval for the regression coefficients using the **prediction-powered percentile bootstrap** method (Kluger et al., 2025; Zrnic, 2024). In particular, we resample both the calibration set and map data points with replacement B times, and for each $1 \leq i \leq B$, we compute the point estimate $\hat{\beta}_{\text{PPI}}^{(i)}$ using the i th resampled dataset. For each $j = 1, \dots, p$, the $(1 - \alpha)$ -level confidence interval for β_j has endpoints that are given by the $\alpha/2$ percentile and $1 - \alpha/2$ percentile of j th entries of the B estimated vectors $\hat{\beta}_{\text{PPI}}^{(1)}, \hat{\beta}_{\text{PPI}}^{(2)}, \dots, \hat{\beta}_{\text{PPI}}^{(B)}$. Larger values of B result in more algorithmically stable confidence intervals, at the cost of increased computational time. Note that an alternative approach to constructing confidence intervals for the estimator in Equation (1) would be to derive an asymptotic normal approximation and variance formula for $\hat{\beta}_{\text{PPI}}$ (e.g., such an approach was developed in Y.-H. Chen and H. Chen (2000); we derive it in Appendix B). However, in this paper we focus on bootstrap-based approaches to constructing confidence intervals because they generalize more readily to nonstandard regression models and can be modified to apply to weighted, stratified, and clustered samples (Kluger et al., 2025).

2.2 Logistic regression

When Y is a binary variable, we can similarly use PPI to estimate the logistic regression coefficients β that give the best fit to the model

$$\mathbb{P}(Y = 1|X) = \frac{1}{1 + e^{-\beta^\top X}}.$$

(We assume that the first element of the vector X is a constant 1, so that the first regression coefficient β_0 is an intercept term.)

The ground truth-only estimator using the n ground truth calibration datapoints is

$$\hat{\beta}_{\text{calib}} = \arg \min_{\beta} \left\{ \sum_{i=1}^n \log(1 + e^{\beta^\top X_i}) - Y_i \beta^\top X_i \right\}.$$

The map-only estimator using the N map datapoints is

$$\hat{\gamma}_{\text{map}} = \arg \min_{\beta} \left\{ \sum_{i=1}^N \log(1 + e^{\beta^\top \hat{X}'_i}) - \hat{Y}'_i \beta^\top \hat{X}'_i \right\}.$$

The estimator using the remote sensing predictions at the n calibration datapoints is

$$\hat{\gamma}_{\text{calib}} = \arg \min_{\beta} \left\{ \sum_{i=1}^n \log(1 + e^{\beta^\top \hat{X}_i}) - \hat{Y}_i \beta^\top \hat{X}_i \right\}.$$

Similar to the linear regression case, the PPI logistic regression coefficient estimate is obtained by plugging these values into Equation (1), and the confidence interval is obtained using the percentile bootstrap. In the case of logistic regression, analytic formulas for an optimal choice of tuning matrix and an estimate of the covariance matrix of $\hat{\beta}_{\text{PPI}}$ are also presented in Appendix B.

2.3 Error-in- Y vs. Error-in- X vs. Error-in-both

PPI for regression coefficient estimation can be applied even when only a subset of the variables are remotely sensed, while the others have ground truth labels at all N locations. We study PPI in three different regression regimes of interest, using the same nomenclature and categorization as Proctor et al. (2023). In the first regime, which we call **error-in- Y** , the investigator wishes to leverage a map product for the response variable, while ground truth data for the covariates are widely available. In the second regime, which we call **error-in- X** , the investigator wishes to leverage a map product for some of the covariates, while ground truth data for the response variable is widely available. In the third regime, which we call **error-in-both**,

ground truth labels are sparsely available for both the response variable and some of the covariates, and the investigator wishes to leverage a map product for these sparsely measured variables.

We consider these three regimes separately for two reasons. First, many existing statistical methods either only apply to the error-in- X regime or only apply to the error-in- Y regime. For example, some earlier variants of PPI (Angelopoulos et al., 2023a,b) are only designed for the error-in- Y regime, while many of the traditional methods in the measurement error literature (Carroll et al., 2006) are only designed for error-in- X regime. However, we emphasize that the variant of PPI presented in this paper can apply to all three regimes (Kluger et al., 2025). Second, the bias of the coefficient is thought to have different behavior and severity in the three regimes. The map-only estimator bias is hypothesized to be least severe in the error-in- Y regime and most severe in the error-in-both regime. For example, if the map error is assumed to be additive noise, the map-only linear regression estimator will have no bias in the error-in- Y regime (Carroll et al., 2006) but in the error-in- X regime it will often be biased towards zero (attenuation bias), and can sometimes be biased away from zero (Kluger et al., 2024; Smeden et al., 2019). In the error-in-both regime, the bias issues from the error-in- Y and error-in- X regimes can aggregate.

Examples All three of these regression settings are commonly seen in the remote sensing literature. We list a few examples here. For error-in- Y , studies have regressed remotely sensed algal blooms against fertilizer use in the US (Taylor and Heal, 2023), and remotely sensed maize and soybean yields against cover crop adoption in the US Corn Belt (Deines et al., 2023). For error-in- X , studies have regressed crop yields against remotely sensed air pollution in China (He et al., 2022), and flood damages against remotely sensed wetland loss in the US (Taylor and Druckenmiller, 2022). For error-in-both, studies have regressed remotely sensed maize and soybean yields against remotely sensed conservation tillage in the US Corn Belt (Deines et al., 2019), and remotely sensed crop greenness against remotely sensed nitrogen oxide levels in several agricultural regions (Lobell et al., 2022).

2.4 Evaluating performance using effective sample size

We use **effective sample size** to compare the effectiveness of regression coefficient estimation methods. Suppose a GT-only confidence interval of width w is generated using n ground truth points. If another estimation method (such as PPI) uses n ground truth points (along with a map product) to generate a confidence interval of width w' , then the effective sample size of the new method is

$$n_{\text{effective}} = n \cdot \left(\frac{w}{w'}\right)^2.$$

This is the number of ground truth points that would be required to generate a GT-only confidence interval of width w' .

3 Examples of regression coefficient estimation

In this section, we apply PPI to estimate regression coefficients in four use cases associating deforestation, tree cover, housing price, and forest cover to other geospatial covariates. We compare point estimates and confidence intervals for the map-only estimator, GT-only estimator, and PPI estimator. Note that our regressions are not meant to contain a comprehensive list of covariates; our examples are primarily a means to illustrate the strengths and weaknesses of each method rather than meant to be interpreted scientifically.

PPI can be applied when the response variable, the covariates, or both are remotely sensed, as long as each remotely sensed variable has a small amount of ground truth data for calibration. In the deforestation and tree cover regressions, the response variable is remotely sensed (error in Y), but ground truth data is widely available for all covariates. In the housing price regression, the response variable has ground truth widely available, but two of the covariates are remotely sensed (error in X). In the forest cover regression, both the response variable and one of the covariates are remotely sensed (error in both X and Y).

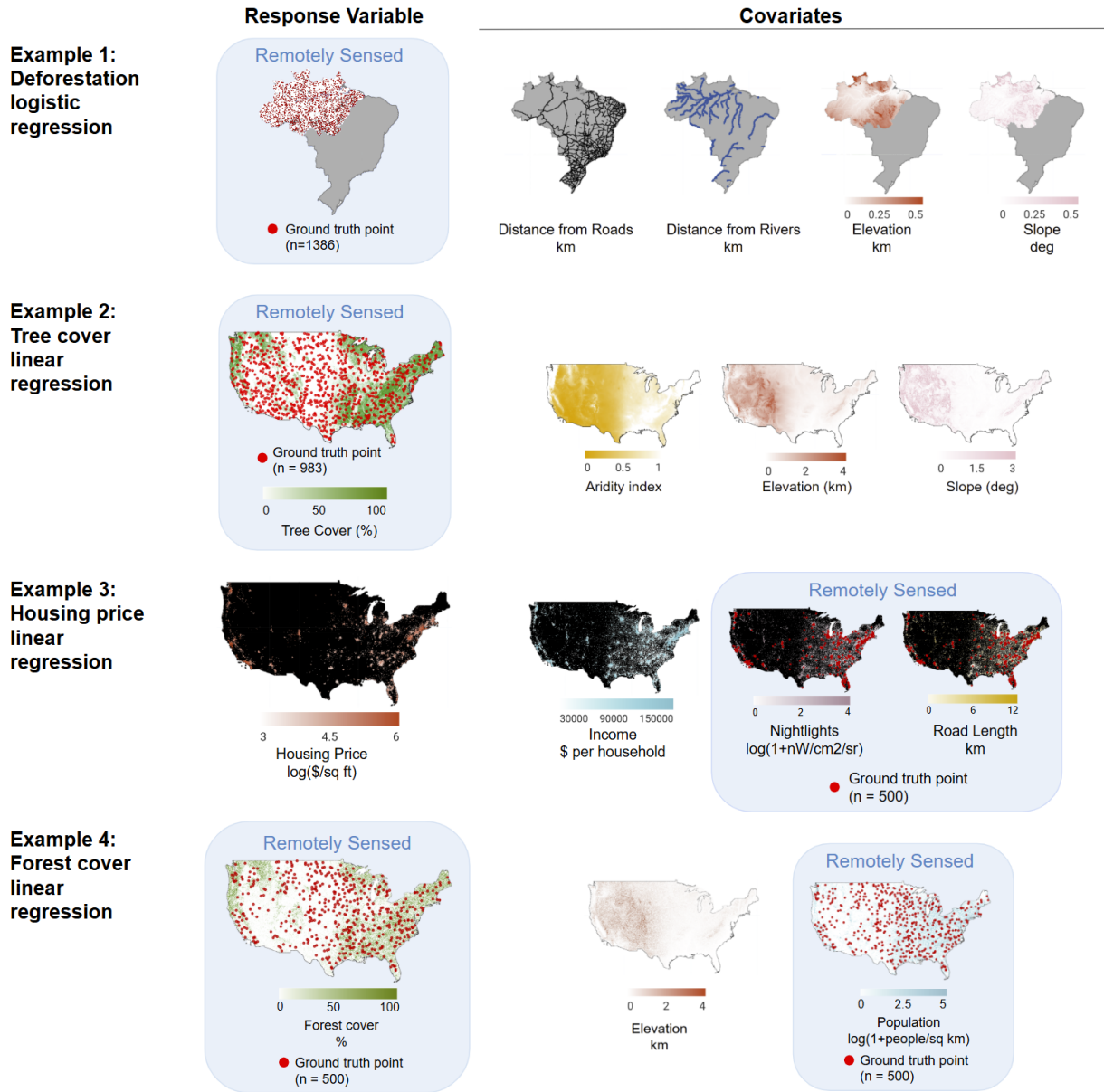


Figure 3: **Response variable and covariates for the four use cases.** We consider use cases with remotely sensed response variable (Examples 1 and 2), remotely sensed covariates (Example 3), or both (Example 4).

3.1 Experimental setup

We first summarize the regression specifications and datasets for the four use cases. Maps for each use case are shown in Figure 3. For more detailed descriptions of the datasets, see Appendix C.

Example 1: Deforestation logistic regression We estimate the logistic regression coefficients for the association between Brazilian Amazon deforestation in 2000–2015 and several covariates: distance from major roads, distance from major rivers, elevation, and slope. We use logistic regression because the response variable (deforested or non-deforested) is binary. Given n data points, the logistic regression model is

$$\log \frac{p}{1-p} = \beta_0 + \beta_{\text{distRoad}} X_{\text{distRoad}} + \beta_{\text{distRiver}} X_{\text{distRiver}} + \beta_{\text{elevation}} X_{\text{elevation}} + \beta_{\text{slope}} X_{\text{slope}}$$

where p is a $n \times 1$ vector of probabilities, X_j is a $n \times 1$ vector of covariate j , and β_j is the scalar logistic regression coefficient for covariate j . We wish to estimate the β_j giving the best fit to the above model. A one-unit increase in covariate j corresponds to a β_j change in the log-odds of the response variable. The scalar β_0 is the intercept, corresponding to the log-odds of the response when the covariates X_j are zero.

The deforestation response variable is remotely sensed while the covariates are treated as ground truth. For remotely sensed deforestation, we create a binary deforestation map product using $N = 963548$ pixels sampled uniformly at random from the NASA Global Forest Cover Change (GFCC) map (Townshend, 2016) (at 30 m resolution) in the study area in 2000 and 2015. For ground truth deforestation, we use $n = 1386$ randomly sampled points from an Amazon deforestation dataset created by Bullock et al. (2020) using time-series analysis of Landsat imagery and high-resolution imagery from Google Earth. For the covariates, we use a map of Brazilian federal roads in 2000 (Castro Victoria et al., 2021), the WWF HydroSHEDS Free Flowing Rivers Network map (Grill et al., 2019), and the NASA Digital Elevation Model (NASA Jet Propulsion Laboratory, 2020).

Example 2: Tree cover linear regression We estimate linear regression coefficients for the association between 2021 tree cover percentage in the contiguous United States and several covariates: aridity index, elevation, and slope. We use linear regression rather than logistic regression because the response variable (tree cover percentage) is continuous rather than binary. Given n data points, the linear regression model is

$$Y = \beta_0 + \beta_{\text{aridity}} X_{\text{aridity}} + \beta_{\text{elevation}} X_{\text{elevation}} + \beta_{\text{slope}} X_{\text{slope}} + \varepsilon$$

where Y is a $n \times 1$ vector of the response variable, X_j is a $n \times 1$ vector of covariate j , and β_j is the scalar linear regression coefficient for covariate j . We wish to estimate the β_j that give the best fit to the above model. A one-unit increase in covariate j corresponds to a β_j change in the response variable. The scalar β_0 is the intercept, corresponding to the response value when the covariates X_j are zero.

The tree cover response variable is remotely sensed while the covariates are treated as ground truth. For remotely sensed tree cover, we use $N = 983238$ map product points sampled uniformly at random from the 2021 USFS Tree Canopy Cover (TCC) product (USDA Forest Service, 2023) at 30 m resolution. For ground truth tree cover, we manually label $n = 983$ high-resolution satellite images from Google Maps (at randomly sampled locations) by visually estimating the proportion of the 30 m by 30 m image that is covered by trees. For the covariates, we use a map of the average Global Aridity Index from 1970-2000 (Trabucco, 2019) and the NASA Digital Elevation Model (NASA Jet Propulsion Laboratory, 2020).

Example 3: Housing price linear regression We estimate linear regression coefficients for the association between housing price in the United States and household income, nighttime light intensity, and road length. The linear regression model is

$$Y = \beta_0 + \beta_{\text{income}} X_{\text{income}} + \beta_{\text{nightlight}} X_{\text{nightlight}} + \beta_{\text{roadLen}} X_{\text{roadLen}} + \varepsilon$$

using similar notation as the previous linear regression example.

Two of the covariates (nightlights and road length) are remotely sensed, but ground truth data is widely available for the response variable (housing price) and one covariate (income). For all variables, we use the MOSAIKS dataset (Rolf et al., 2021) which contains a population-weighted random sample of points in the

United States at roughly 1 km resolution. There are $N = 46418$ points that have both ground truth and remotely sensed values for housing price (log dollars per square foot), household income (dollars), nighttime light intensity ($\log(1 + nW/\text{cm}^2/\text{sr})$), and road length (km).

For housing price and income, we use the ground truth values for all 46418 points. For nightlights and road length, we take a uniform random subsample of $n = 500$ points as the ground truth calibration set (and use remotely sensed values for the remaining points). For the GT-only method, we use only the $n = 500$ ground truth points for all four variables. We also compare the regression coefficient point estimates from our methods against the “true coefficients” computed by running linear regression on the full set of 46418 ground truth points for all four variables.

Example 4: Forest cover linear regression We estimate linear regression coefficients for the association between forest cover in the United States and two covariates: elevation and population. The linear regression model is

$$Y = \beta_0 + \beta_{\text{elevation}}X_{\text{elevation}} + \beta_{\text{population}}X_{\text{population}} + \varepsilon$$

using similar notation as the previous linear regression examples.

Both the response variable (forest cover) and one of the covariates (population) are remotely sensed, while ground truth data is widely available for the other covariate (elevation). Similar to the previous example, we use the MOSAIKS dataset (Rolf et al., 2021). The dataset also provides a uniformly-weighted random sample of points in the United States at ~ 1 km resolution. After removing points with missing variables, there are $N = 67968$ points that have both ground truth and remotely sensed values for forest cover percentage, elevation (km), and population ($\log(1 + \text{people})/\text{km}^2$).

For elevation, we use the ground truth values for all 67968 points. For forest cover and population, we take a uniform random subsample of $n = 500$ points as the ground truth calibration set (and use remotely sensed values for the remaining points). For the GT-only method, we use only the $n = 500$ ground truth points for all three variables. We also compare the regression coefficient point estimates from our methods against the “true coefficients” computed by running linear regression on the full set of 67968 ground truth points for all four variables.

3.2 Results

The regression coefficient point estimates and 95% confidence intervals for all four use cases are shown in Figure 4. We compare results for the map-only, GT-only, and PPI estimators. (For all experiments in this section, we use $B = 2000$ bootstrap iterations to construct PPI confidence intervals.)

Map-only estimates are biased and their confidence intervals are too narrow. For all coefficients, the map-only confidence intervals are much narrower than those for GT-only and PPI. Unlike the GT-only and PPI intervals, the map-only intervals are not guaranteed with 95% probability to contain the true coefficients (i.e., the GT-only coefficients we would compute if we had access to ground truth data at every pixel).

For instance, in Example 1 (deforestation logistic regression), the map-only estimate for the distance from river coefficient has a very narrow confidence interval around -0.002 and falls outside the PPI interval. Meanwhile, the GT-only and PPI confidence intervals are much wider, capturing the true uncertainty in the data, and both intersect with zero. Using only the maps would lead us to conclude that there is a significantly negative association between deforestation and distance from the nearest river, while the two methods that use ground truth points suggest that there may be no association.

In Examples 3 and 4 (housing price and forest cover linear regressions), we have access to the true coefficients computed from the MOSAIKS dataset. We find that for all but one coefficient, the map-only confidence interval does not contain the true coefficient. We compute the bias (in percentages) of each map-only coefficient point estimate by subtracting the true coefficient from the map-only coefficient, then dividing the result by the true coefficient. Negative values of bias indicate the map-only coefficient is biased toward zero, and positive values indicate the map-only coefficient is biased away from zero. In our examples, the biases of the map-only coefficients range from -18.9% to $+64.3\%$.

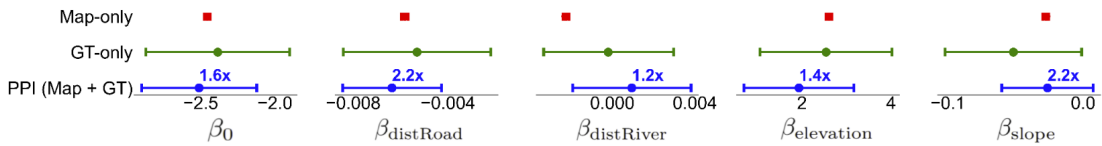
Regression coefficient estimates

Key

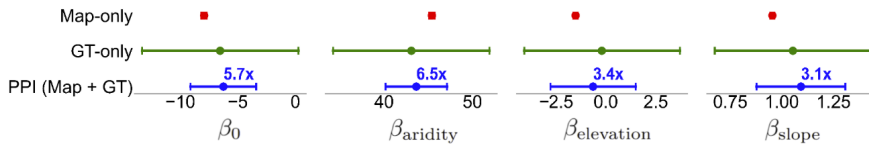
-18.9% = Bias in magnitude of map-only estimate

6.2x = PPI effective sample size improvement over GT-only

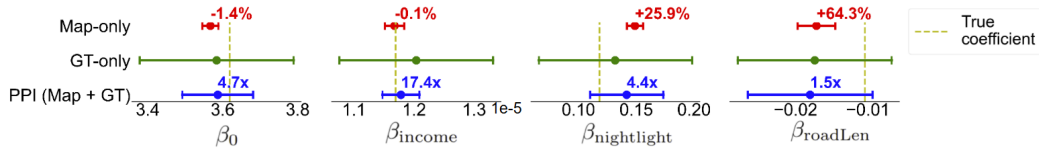
Example 1: Deforestation logistic regression



Example 2: Tree cover linear regression



Example 3: Housing price linear regression



Example 4: Forest cover linear regression

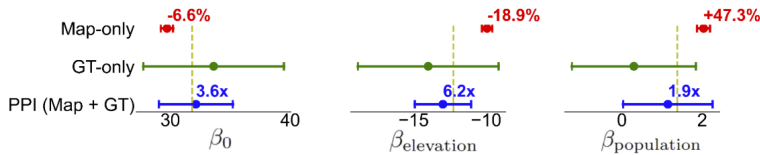


Figure 4: **Regression coefficient point estimates and 95% confidence intervals for the four use cases.** PPI results in smaller 95% confidence intervals than using ground truth only. PPI effective sample size improvements (relative to GT-only) are shown in blue. For the two examples where the true coefficient is known, the bias in magnitude of each map-only estimate is shown in red.

The single unbiased map-only estimate is for income in the housing price linear regression. While there are no guarantees, map-only estimates could happen to be unbiased for a variety of reasons. In the case of an error-in- X linear regression, the estimated coefficients corresponding to a covariate for which only ground truth observations are used will be unbiased if that covariate is uncorrelated with both the map predictions and the map prediction errors of the other covariates (see Formula (5) in Kluger et al. (2024)). We suspect the map-only estimate for the income coefficient is unbiased in our experiment because (i) ground truth income data is used for all samples, (ii) income is uncorrelated with the errors in the nightlights and road length predictions, and (iii) income is only weakly correlated with the nightlights and road length predictions themselves.

PPI uses ground truth data to correct for map bias. PPI gives an unbiased estimator, and the PPI confidence intervals have theoretical guarantees of containing the true coefficients with 95% probability. In Examples 3 and 4, the GT-only and PPI confidence intervals contain all of the true coefficients. PPI successfully uses the ground truth calibration set to correct for bias from the map product and account for uncertainty due to map product errors.

PPI confidence intervals outperform the GT-only method. PPI uses the map product along with the ground truth to reduce uncertainty in the coefficient estimates, resulting in significantly smaller confidence intervals and larger effective sample sizes compared to the GT-only method. In our experiments, the PPI effective sample sizes range from $1.2\times$ to $17.4\times$ the ground truth calibration set size n .

The largest PPI effective sample size improvement ($17.4\times$) is for the income coefficient in Example 3. We suspect that this is because the map-only income coefficient was essentially unbiased, so the PPI estimator for this coefficient involved a very small bias correction term, and therefore was similar to the low variance map-only estimator. The next largest PPI effective sample size improvements are for the elevation coefficient ($6.2\times$) in Example 4 and the aridity coefficient ($6.5\times$) and intercept ($5.7\times$) in Example 2 (tree cover linear regression). In contrast, adding map data did not reduce the confidence interval size significantly for the distance to river ($1.2\times$) and elevation ($1.4\times$) coefficients in Example 1.

4 Simulating the role of map error

To understand the effect of map product quality on PPI regression coefficient estimates, we simulate adding noise and bias to the map products in Example 4 (forest cover linear regression) from the previous section. We compare the resulting point estimates and 95% coefficient confidence intervals at different levels of map noise and bias using map-only, GT-only, and PPI estimators.

4.1 Experimental Setup

Similar to Example 4, we use the MOSAIKS dataset to regress forest cover against elevation and population, where forest cover and population are remotely sensed. We use the same $n = 500$ randomly selected ground truth points as in the original experiment. However, instead of using the MOSAIKS map product datasets for forest cover and population, we take the full MOSAIKS ground truth dataset (67968 points) and use it to create simulated “map products” with different levels of noise and bias. We experiment with adding noise or bias to the population map (error-in- X), the forest cover map (error-in- Y), or both (error-in-both). No error is added to the elevation dataset.

Simulating Noise For the ground truth population covariate X_{pop} , we define “noise at level c ” as additive Gaussian noise with mean zero and standard deviation equal to c times $\sigma_{X_{\text{pop}}}$, the standard deviation of all X_{pop} values in the full ground truth dataset. The resulting simulated map product population value at each point is

$$X_{\text{pop}}^{\text{map}} = X_{\text{pop}} + c \cdot \mathcal{N}(0, \sigma_{X_{\text{pop}}}^2).$$

Similarly, for the forest cover response variable Y , the simulated map product value at each point is

$$Y^{\text{map}} = Y + c \cdot \mathcal{N}(0, \sigma_Y^2).$$

We experiment with noise levels c from 0 to 1 at increments of 0.1. When $c = 0$, the simulated map is the same as the full ground truth map.

Simulating Bias To simulate bias for the ground truth population covariate X_{pop} , we fit a square root regression relating X_{pop} to the corresponding MOSAICS map product values X'_{pop} , using all $N = 67968$ points. We obtain the regression $\hat{X}'_{\text{pop}} = 1.74\sqrt{X_{\text{pop}}} - .22$. We can treat \hat{X}'_{pop} as a biased prediction for X_{pop} . We choose a square root curve as an example to simulate nonlinear bias in map products, as we often observe machine learning predictions to saturate at high values of a variable. (Another model of bias, linear mean reversion, is explored through simulations in Appendix G.)

Then we create a simulated map product with “bias level c ” by interpolating between X_{pop} and \hat{X}'_{pop} to get

$$X_{\text{pop}}^{\text{map}} = c\hat{X}'_{\text{pop}} + (1 - c)X_{\text{pop}}.$$

Similarly, for the forest cover response variable Y , we use the MOSAICS map product Y' to fit the square root regression $\hat{Y}' = 7.90\sqrt{Y} - 3.20$. The simulated map product value at each point is

$$Y^{\text{map}} = c\hat{Y}' + (1 - c)Y.$$

We experiment with bias levels c from 0 to 1 at increments of 0.1. When $c = 0$, the simulated map is the same as the full ground truth map. When $c = 1$, the simulated map is the same as the biased prediction \hat{X}'_{pop} or \hat{Y}' .

4.2 Results

The coefficient point estimates and 95% confidence intervals at each noise and bias level are shown in Figure 5. We compare results for the map-only, GT-only, and PPI estimators. (For all experiments in this section, we use $B = 200$ bootstrap iterations to construct PPI confidence intervals.)

GT-only confidence interval is wide. First, the GT-only point estimate and confidence interval stay constant regardless of noise and bias, because they use a constant set of ground truth points. The confidence interval contains the true coefficients for both covariates (-12 for elevation and 1.4 for population). However, due to the small number of ground truth points ($n = 500$), the GT-only interval for β_{pop} also contains zero, so it does not detect a statistically significant association between forest cover and population. The GT-only interval is wider than the PPI and map-only intervals; exactly how much wider depends on the noise and bias levels.

Both noise and bias lead to biased map-only estimates. Second, the map-only estimates suffer from bias when either noise or bias is added to the variables. In the noise experiments, the map-only estimates for β_{pop} and $\beta_{\text{elevation}}$ become biased when there is noise in X_{pop} . As noise increases, the map-only estimates for β_{pop} decrease in magnitude and become biased toward zero, because additive Gaussian noise in a covariate results in attenuation bias in the corresponding regression coefficient (see Section 2.3). The map-only estimates for $\beta_{\text{elevation}}$ conversely become larger in magnitude as noise in X_{pop} increases.

Furthermore, the map-only confidence intervals are narrow because the number of map product points is large ($N = 67968$), but unlike the PPI intervals, they fail to capture the true estimation uncertainties due to map imperfections. The confidence intervals for β_{pop} do not contain the true coefficient for X_{pop} noise levels $c \geq 0.4$ (corresponding to $R^2 \leq 0.92$ for the simulated population map). The confidence intervals for $\beta_{\text{elevation}}$ do not contain the true coefficient for X_{pop} noise levels $c \geq 0.6$ ($R^2 \leq 0.82$). By X_{pop} noise levels of $c = 0.8$ ($R^2 = 0.68$), the map-only estimate of β_{pop} is roughly half of the true coefficient. In contrast, noise in Y (forest cover) does not result in biased map-only estimates, because zero-centered noise in a response variable does not bias regression coefficients.

Simulating the Role of Map Error

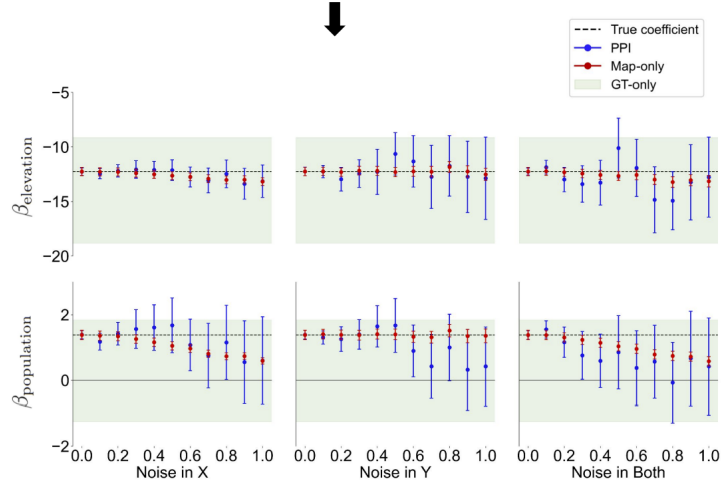
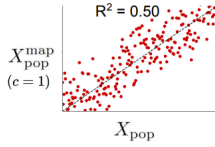
Regression specification

$$Y = \beta_0 + \beta_{\text{elevation}} X_{\text{elevation}} + \beta_{\text{population}} X_{\text{population}} + \varepsilon$$

Varying simulated noise

$$X_{\text{pop}}^{\text{map}} = X_{\text{pop}} + c \cdot \mathcal{N}(0, \sigma_{X_{\text{pop}}}^2)$$

$$Y^{\text{map}} = Y + c \cdot \mathcal{N}(0, \sigma_Y^2)$$



Varying simulated bias

$$X_{\text{pop}}^{\text{map}} = c\hat{X}'_{\text{pop}} + (1-c)X_{\text{pop}}$$

$$Y^{\text{map}} = c\hat{Y}' + (1-c)Y$$

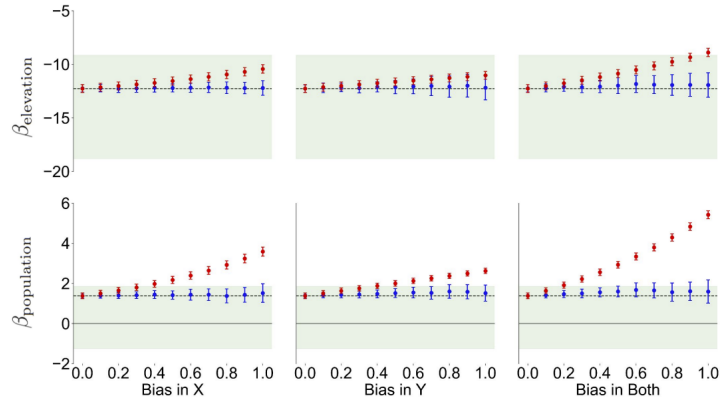
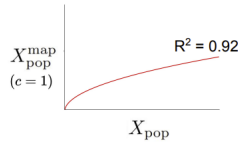


Figure 5: **Simulation estimating forest cover linear regression coefficient 95% confidence intervals under different levels of map noise and map bias.** In the bias simulations, \hat{X}'_{pop} and \hat{Y}' are nonlinearly biased proxies for true X_{pop} and Y . Even with map noise or bias, PPI gives unbiased estimates with narrower confidence intervals than the GT-only method. Map-only estimates become increasingly biased as noise in the simulated map products for X_{pop} increases or bias in the simulated map products for X_{pop} or Y increases. We also display the R^2 coefficient of determination for $X_{\text{pop}}^{\text{map}}$ at $c = 1$ noise and bias levels.

Whether bias is in X_{pop} , Y , or both, the map-only estimates become biased. Similar to in the noise experiments, when we add bias the map-only confidence intervals remain narrow but fail to capture the actual estimation uncertainty. The map-only confidence intervals do not contain the true coefficient for β_{pop} at bias levels $c \geq 0.2$ ($R^2 \leq 0.997$ for simulated population and forest cover maps) or the true coefficient for $\beta_{\text{elevation}}$ at bias levels $c \geq 0.4$ ($R^2 \leq 0.987$ for X_{pop} and $R^2 \leq 0.988$ for Y). When the bias level of X_{pop} is at $c = 1$ (in other words, $X_{\text{pop}}^{\text{map}} = \hat{X}'_{\text{pop}}$)—corresponding to $R^2 = 0.92$ of the map compared to ground truth—treating the map as if it were 100% accurate would nearly double the estimate for β_{pop} . The direction of bias in coefficient estimates varies depending on the type of bias in the map and can be difficult to predict in general. In our bias experiments, the map-only estimates for β_{pop} become biased away from zero while those for $\beta_{\text{elevation}}$ become biased toward zero.

We reported the R^2 of map products above because R^2 is a common evaluation metric for remote sensing maps (MSE is another common metric, but its values are variable-specific). We draw attention to the fact that map R^2 can be high (> 0.9)—in other words, the map appears very accurate—but the map-only estimator still yields significantly biased coefficients.

Performance of PPI. Finally, our simulations allow us to see clearly the advantages and limitations of PPI. At almost all noise and bias levels across experiments, the PPI confidence intervals contain the true coefficients for both covariates. (The only exception is noise level $c = 0.8$ for “noise in both,” corresponding to $R^2 = 0.68$ for X_{pop} and $R^2 = 0.36$ for Y .) This is expected, as PPI uses the small set of ground truth points to correct for error and quantify uncertainty in the map product, and the PPI confidence intervals are guaranteed to contain the true coefficient with 95% probability.

In contrast to using GT-only, PPI estimates β_{pop} and $\beta_{\text{elevation}}$ much more precisely, allowing us to correctly conclude that there is a positive association between forest cover and population. The PPI estimate for β_{pop} is only indistinguishable from zero at noise levels of $c \geq 0.7$ in X_{pop} ($R^2 \leq 0.75$), $c \geq 0.7$ in Y ($R^2 \leq 0.51$), or $c \geq 0.4$ in both ($R^2 \leq 0.92$ for X_{pop} and $R^2 \leq 0.84$ for Y). The PPI estimates are statistically significant at all bias levels in our experiment.

The effectiveness of PPI is dependent on the quality of the map product. When the noise or bias level is low, the PPI intervals are significantly smaller than the GT-only interval, because the simulated map product is close to ground truth and provides useful information for estimating the regression coefficients. As the noise level increases and the quality of the map deteriorates, the PPI intervals grow wider, approaching the GT-only interval. For example, when the noise level is $c = 0.2$ in both X_{pop} and Y ($R^2 = 0.98$ for X_{pop} and $R^2 = 0.96$ for Y), the PPI effective sample size outperforms the GT-only method by a factor of $18.8\times$ for elevation and $11.2\times$ for population. When the noise level increases to $c = 0.9$ ($R^2 = 0.59$ for X_{pop} and $R^2 = 0.19$ for Y), the PPI effective sample size only outperforms the GT-only method by $2.0\times$ for elevation and $1.1\times$ for population.

As the bias level increases, the PPI intervals grow wider but remain significantly smaller than the GT-only interval, because the biased map (which uses a square root transformation of the true variable values) still contains significant information about the true population and forest cover values. For example, when the bias level is $c = 0.2$ in both X_{pop} and Y ($R^2 = 0.997$ for both), the PPI effective sample size outperforms the GT-only method by a factor of $133\times$ for elevation and $77\times$ for population. When the bias level increases to $c = 0.9$ ($R^2 = 0.94$ for both), the PPI effective sample size only outperforms the GT-only method by $20\times$ for elevation and $11\times$ for population.

5 Discussion

Using remote sensing-based maps to draw scientific inferences requires uncertainty quantification and propagation of uncertainty to downstream analyses — otherwise, we risk making, in the words of McRoberts (2011), just pretty pictures. In this work, we applied prediction-powered inference, using remote sensing map products along with a small amount of ground truth data, to estimate regression coefficients, while correctly taking into account the errors in the map products. We find that PPI estimates have narrower confidence intervals than the GT-only estimates. Unlike map-only estimates using the map product alone, the PPI estimates are guaranteed to be unbiased.

Bias is the main issue for map-only estimates. Our experiments illustrate that a map-only regression coefficient estimate without bias correction can yield incorrect inferences. We see this clearly in our examples with MOSAICS data in which we know the true coefficients. In Example 3 (housing price linear regression), the map-only estimator underestimates the intercept and overestimates the magnitude of the nightlight and road length coefficients. In Example 4 (forest cover linear regression), the map-only estimator underestimates the intercept, underestimates the magnitude of the elevation coefficient, and overestimates the magnitude of the population coefficient. In our map error simulations with forest cover linear regression (Section 4), the map-only estimates of elevation and population coefficients become increasingly biased as we add noise in X or add bias in X or Y to the simulated maps. In all cases, the map-only estimator has very narrow confidence intervals that give a false sense of certainty. To address the bias of map-only estimators and under-coverage of their confidence intervals, we use PPI to incorporate ground truth data into our estimates.

Performance of PPI. PPI uses the ground truth calibration data to correct the map product, resulting in unbiased regression coefficient estimates. Unlike map-only estimates, the PPI confidence intervals are guaranteed to have the appropriate coverage probability (e.g. 95%) for the true coefficient of interest. This is seen in Examples 3 and 4 (housing price and forest cover linear regressions), where the PPI confidence intervals contain the true coefficients for all covariates. In our map error simulations, all but one of the PPI confidence intervals contain the true coefficient, even when there is a high level of noise or bias in the map.

The width of PPI confidence intervals compared to the GT-only method depends on the quality of the map product. If the map product is fairly accurate (i.e., the map product predictions (\hat{X}, \hat{Y}) are close to the ground truth values (X, Y)), the PPI regression coefficient confidence intervals are generally substantially smaller than the GT-only intervals. However, if the map product is low quality, the PPI estimator does not offer a significant advantage over the GT-only estimator. For instance, in our map noise simulations, the PPI confidence intervals become wider and approach the GT-only confidence intervals as noise increases and the quality of the map deteriorates. We also see in our experiments that the performance of PPI varies for different covariates. For instance, in Example 3, the PPI effective sample size outperforms the GT-only estimator by a factor of $17.4\times$ for the income covariate, while the road length covariate has a more modest $1.5\times$ improvement.

Recommendations for map producers and users. Ultimately, the best methods combine map products with ground truth to yield the narrowest intervals (highest certainty). We recommend that producers of machine learning-generated remote sensing maps use a randomly sampled holdout ground truth dataset if they wish to estimate and construct confidence intervals for regression coefficients. The criterion for this holdout set is that the model, including during hyperparameter tuning, was not trained on it; a standard test set would be adequate, provided that it is randomly sampled and representative of the inference population. Map producers should release this ground truth data and details of its sampling scheme alongside their map product to make their map suitable for downstream scientific inferences. When there are privacy concerns for releasing ground truth data, map producers can alternatively collaborate with map users on federated approaches for PPI, such as those described in Miao and Lu (2024). In the absence of this, we recommend that map users generate their own ground truth data for the variable of interest if possible (e.g., through manual inspection of remote sensing imagery).

Limitations. PPI is limited to areas in which ground truth data is available. However, this would be necessary for any method that does not make further assumptions about the errors of the machine-learning model. Furthermore, the calibration dataset must be a sample from the ground-truth distribution of interest (this ensures that the PPI and GT-only estimators will both be unbiased). If the ground truth data sampling process is biased, the regression coefficient estimates using these ground truth points may not reflect the true relationships between variables.

Together, these attributes mean that such methods may be especially straightforward to use when ground truth data can be generated *de novo*, such as from human inspection of available satellite imagery, and more challenging to use when ground truth data requires field data collection or survey data collection.

The current theory for PPI focuses on the i.d.d. case, whereas in remote sensing we would usually have a fixed area of interest and then randomly sample a subset of the points in the area as the calibration set

(*design-based inference*). In survey sampling it is known that the former often approximates the latter well when the sample is small relative to the total population, but admittedly this connection has not yet been made explicit for PPI.

While PPI applies to settings where the ground truth sample is collected from a weighted random sample, a stratified random sample, or a clustered random sample (Kluger et al., 2025), we note that this work does not explore these common settings. In addition, PPI can be used for a variety of regression models beyond generalized linear models such as quantile regression (e.g., Kluger et al. (2025) and Miao and Lu (2024)), although due to space constraints we only consider generalized linear models in this paper.

Acknowledgments

This material is based upon work supported by the U.S. Department of Energy, Office of Science, Office of Advanced Scientific Computing Research, Department of Energy Computational Science Graduate Fellowship under Award Number(s) DE-SC0023112. This report was prepared as an account of work sponsored by an agency of the United States Government. Neither the United States Government nor any agency thereof, nor any of their employees, makes any warranty, express or implied, or assumes any legal liability or responsibility for the accuracy, completeness, or usefulness of any information, apparatus, product, or process disclosed, or represents that its use would not infringe privately owned rights. Reference herein to any specific commercial product, process, or service by trade name, trademark, manufacturer, or otherwise does not necessarily constitute or imply its endorsement, recommendation, or favoring by the United States Government or any agency thereof. The views and opinions of authors expressed herein do not necessarily state or reflect those of the United States Government or any agency thereof.

References

- Alix-Garcia, Jennifer and Daniel L Millimet (2023). “Remotely incorrect? Accounting for nonclassical measurement error in satellite data on deforestation”. In: *Journal of the Association of Environmental and Resource Economists* 10.5, pp. 1335–1367.
- Angelopoulos, Anastasios N and Stephen Bates (2023). “Conformal prediction: A gentle introduction”. In: *Foundations and Trends® in Machine Learning* 16.4, pp. 494–591.
- Angelopoulos, Anastasios N, John C Duchi, and Tijana Zrnic (2023a). “PPI++: Efficient prediction-powered inference”. In: *arXiv preprint arXiv:2311.01453*.
- Angelopoulos, Anastasios N et al. (2023b). “Prediction-powered inference”. In: *Science* 382.6671, pp. 669–674.
- Arima, Eugenio Y et al. (2016). “Explaining the fragmentation in the Brazilian Amazonian forest”. In: *Journal of Land Use Science* 11.3, pp. 257–277.
- Baccini, A. et al. (2012). “Estimated carbon dioxide emissions from tropical deforestation improved by carbon-density maps”. In: *Nature Climate Change* 2.3, pp. 182–185.
- Bastin, Jean-François et al. (2017). “The extent of forest in dryland biomes”. In: *Science* 356.6338, pp. 635–638.
- Berdugo, Miguel et al. (2020). “Global ecosystem thresholds driven by aridity”. In: *Science* 367.6479, pp. 787–790.
- Brandão Jr, Amintas O and Carlos M Souza Jr (2006). “Mapping unofficial roads with Landsat images: a new tool to improve the monitoring of the Brazilian Amazon rainforest”. In: *International Journal of Remote Sensing* 27.1, pp. 177–189.
- Bullock, Eric L et al. (2020). “Satellite-based estimates reveal widespread forest degradation in the Amazon”. In: *Global Change Biology* 26.5, pp. 2956–2969.
- Card, Don (1982). “Using Known Map Category Marginal Frequencies to Improve Estimates of Thematic Map Accuracy”. In: *Photogrammetric Engineering and Remote Sensing* 48.3, pp. 431–439.
- Carroll, Raymond J. et al. (2006). *Measurement Error in Nonlinear Models: A Modern Perspective, Second Edition*. 2nd. London: Chapman and Hall/CRC. DOI: [10.1201/9781420010138](https://doi.org/10.1201/9781420010138).
- Castro Victoria, Daniel de et al. (2021). “Transport cost to port through Brazilian federal roads network: Dataset for years 2000, 2005, 2010 and 2017”. In: *Data in brief* 36, p. 107070.

- Chen, Yi-Hau and Hung Chen (2000). “A unified approach to regression analysis under double-sampling designs”. In: *Journal of the Royal Statistical Society Series B: Statistical Methodology* 62.3, pp. 449–460.
- Cochran, W.G. (1977). *Sampling Techniques*. Wiley Series in Probability and Statistics. Wiley. ISBN: 9780471162407. URL: <https://books.google.com/books?id=8Y4QAQAIAAJ>.
- Deines, Jillian M, Sherrie Wang, and David B Lobell (Dec. 2019). “Satellites reveal a small positive yield effect from conservation tillage across the US Corn Belt”. In: *Environmental Research Letters* 14.12, p. 124038.
- Deines, Jillian M et al. (2023). “Recent cover crop adoption is associated with small maize and soybean yield losses in the United States”. In: *Global change biology* 29.3, pp. 794–807.
- Etter, Andrés et al. (2006). “Regional patterns of agricultural land use and deforestation in Colombia”. In: *Agriculture, ecosystems & environment* 114.2-4, pp. 369–386.
- Fisch, Adam et al. (2024). “Stratified Prediction-Powered Inference for Hybrid Language Model Evaluation”. In: *arXiv preprint arXiv:2406.04291*.
- Gallego, F Javier (2004). “Remote sensing and land cover area estimation”. In: *International Journal of Remote Sensing* 25.15, pp. 3019–3047.
- Gordon, Matthew et al. (2023). “Remote control: Debiasing remote sensing predictions for causal inference”. In: *Proc. Int. Conf. Learn. Represent. Workshops*. 22.
- Grill, Günther et al. (2019). “Mapping the world’s free-flowing rivers”. In: *Nature* 569.7755, pp. 215–221.
- Hansen, M. C. et al. (2013). “High-Resolution Global Maps of 21st-Century Forest Cover Change”. In: *Science* 342.6160, pp. 850–853.
- He, Liyin et al. (2022). “Marked impacts of pollution mitigation on crop yields in China”. In: *Earth’s Future* 10.11, e2022EF002936.
- Jain, Meha (2020). “The benefits and pitfalls of using satellite data for causal inference”. In: *Review of Environmental Economics and Policy*.
- Kirby, Kathryn R et al. (2006). “The future of deforestation in the Brazilian Amazon”. In: *Futures* 38.4, pp. 432–453.
- Kluger, Dan M., David B. Lobell, and Art B. Owen (2024). “Biases in estimates of air pollution impacts: the role of omitted variables and measurement errors”. In: *arXiv:2310.08831 [stat.AP]*. doi.org/10.48550/arXiv.2310.08831.
- Kluger, Dan M. et al. (2025). “Prediction-Powered Inference with Imputed Covariates and Nonuniform Sampling”. In: *arXiv:2501.18577 [stat.ME]*. <https://doi.org/10.48550/arXiv.2501.18577>.
- Laurance, William F et al. (2002). “Predictors of deforestation in the Brazilian Amazon”. In: *Journal of biogeography* 29.5-6, pp. 737–748.
- Lobell, David B, Stefania Di Tommaso, and Jennifer A Burney (2022). “Globally ubiquitous negative effects of nitrogen dioxide on crop growth”. In: *Science advances* 8.22, eabm9909.
- Mayor, Jordan R et al. (2017). “Elevation alters ecosystem properties across temperate treelines globally”. In: *Nature* 542.7639, pp. 91–95.
- McRoberts, Ronald E. (2011). “Satellite image-based maps: Scientific inference or pretty pictures?” In: *Remote Sensing of Environment* 115.2, pp. 715–724. ISSN: 0034-4257.
- McRoberts, Ronald E. et al. (2022). “On the model-assisted regression estimators using remotely sensed auxiliary data”. In: *Remote Sensing of Environment* 281, p. 113168. ISSN: 0034-4257. DOI: <https://doi.org/10.1016/j.rse.2022.113168>. URL: <https://www.sciencedirect.com/science/article/pii/S0034425722002826>.
- Miao, Jiacheng and Qiongshi Lu (2024). “Task-Agnostic Machine-Learning-Assisted Inference”. In: *38th Conference on Neural Information Processing Systems*. <https://arxiv.org/abs/2405.20039>. NeurIPS.
- NASA Jet Propulsion Laboratory (2020). “NASADEM Merged DEM Global 1 arc second V001 [Data set]”. In: *NASA EOSDIS Land Processes DAAC*.
- Olofsson, Pontus et al. (2013). “Making better use of accuracy data in land change studies: Estimating accuracy and area and quantifying uncertainty using stratified estimation”. In: *Remote Sensing of Environment* 129, pp. 122–131.
- Olofsson, Pontus et al. (2014). “Good practices for estimating area and assessing accuracy of land change”. In: *Remote sensing of Environment* 148, pp. 42–57.
- Olofsson, Pontus et al. (2020). “Mitigating the effects of omission errors on area and area change estimates”. In: *Remote Sensing of Environment* 236, p. 111492.

- Perz, Stephen G et al. (2007). “Unofficial road building in the Brazilian Amazon: dilemmas and models for road governance”. In: *Environmental Conservation* 34.2, pp. 112–121.
- Potapov, Peter et al. (2022). “Global maps of cropland extent and change show accelerated cropland expansion in the twenty-first century”. In: *Nature Food* 3.1, pp. 19–28.
- Proctor, Jonathan, Tamma Carleton, and Sandy Sum (2023). *Parameter recovery using remotely sensed variables*. Tech. rep. National Bureau of Economic Research.
- Rolf, Esther et al. (2021). “A generalizable and accessible approach to machine learning with global satellite imagery”. In: *Nature Communications* 12.1, p. 4392.
- Rosa, Isabel MD et al. (2013). “Predictive modelling of contagious deforestation in the Brazilian Amazon”. In: *PloS one* 8.10, e77231.
- Sandel, Brody and Jens-Christian Svenning (2013). “Human impacts drive a global topographic signature in tree cover”. In: *Nature Communications* 4.1, p. 2474.
- Särndal, Carl-Erik, Bengt Swensson, and Jan Wretman (2003). *Model assisted survey sampling*. Springer Science & Business Media.
- Smeden, Maarten van, Timothy L Lash, and Rolf H H Groenwold (Dec. 2019). “Reflection on modern methods: five myths about measurement error in epidemiological research”. In: *International Journal of Epidemiology* 49.1, pp. 338–347. ISSN: 0300-5771. DOI: [10.1093/ije/dyz251](https://doi.org/10.1093/ije/dyz251). eprint: <https://academic.oup.com/ije/article-pdf/49/1/338/32995679/dyz251.pdf>. URL: <https://doi.org/10.1093/ije/dyz251>.
- Stehman, Stephen V (2000). “Practical Implications of Design-Based Sampling Inference for Thematic Map Accuracy Assessment”. In: *Remote Sensing of Environment* 72.1, pp. 35–45. ISSN: 0034-4257. DOI: [https://doi.org/10.1016/S0034-4257\(99\)00090-5](https://doi.org/10.1016/S0034-4257(99)00090-5). URL: <https://www.sciencedirect.com/science/article/pii/S0034425799000905>.
- (2013). “Estimating area from an accuracy assessment error matrix”. In: *Remote Sensing of Environment* 132, pp. 202–211.
- Stehman, Stephen V and Giles M Foody (2019). “Key issues in rigorous accuracy assessment of land cover products”. In: *Remote Sensing of Environment* 231, p. 111199.
- Taylor, Charles A and Hannah Druckenmiller (2022). “Wetlands, flooding, and the clean water act”. In: *American Economic Review* 112.4, pp. 1334–1363.
- Taylor, Charles A and Geoffrey Heal (2023). “Fertilizer and Algal Blooms”. In: *Risks in Agricultural Supply Chains*, p. 83.
- Townshend, J (2016). “Global Forest cover change (GFCC) tree cover multi-year global 30 m V003”. In: *NASA EOSDIS Land Processes DAAC*, pp. 176–184.
- Trabucco, Antonio (2019). “Global aridity index and potential evapotranspiration (ET0) climate database v2”. In: *CGIAR Consort Spat Inf.*
- United Nations Satellite Imagery and Geospatial Data Task Team (2017). *Earth Observations for Official Statistics*. United Nations.
- USDA Forest Service (2023). “USFS Tree Canopy Cover v2021.4 (Conterminous United States and South-eastern Alaska)”. In: *Salt Lake City, Utah*.
- USDA NASS (2024). “USDA national agricultural statistics service cropland data layer”. In: *USDA-NASS, Washington, DC*.
- Vaart, A. W. van der (1998). *Asymptotic Statistics*. Cambridge Series in Statistical and Probabilistic Mathematics. Cambridge University Press.
- Valle, Denis, Rafael Izbicki, and Rodrigo Vieira Leite (2023). “Quantifying uncertainty in land-use land-cover classification using conformal statistics”. In: *Remote Sensing of Environment* 295, p. 113682.
- Valle, Denis et al. (2024). “An automated procedure to determine construction year of roads in forested landscapes using a least-cost path and a Before-After Control-Impact approach”. In: *Remote Sensing in Ecology and Conservation* 10.3, pp. 388–400.
- Venter, Zander S et al. (2022). “Global 10 m land use land cover datasets: A comparison of dynamic world, world cover and esri land cover”. In: *Remote Sensing* 14.16, p. 4101.
- Venter, Zander S et al. (2024). ““Uncertainty audit” for ecosystem accounting: Satellite-based ecosystem extent is biased without design-based area estimation and accuracy assessment”. In: *Ecosystem Services* 66, p. 101599.

- Vovk, Vladimir, Alexander Gammerman, and Glenn Shafer (2005). *Algorithmic learning in a random world*. Vol. 29. Springer.
- Wang, Mengqiu et al. (2019). “The great Atlantic Sargassum belt”. In: *Science* 365.6448, pp. 83–87.
- Williams, A Park et al. (2010). “Forest responses to increasing aridity and warmth in the southwestern United States”. In: *Proceedings of the National Academy of Sciences* 107.50, pp. 21289–21294.
- World Bank Group (2018). *Mainstreaming the use of remote sensing data and applications in operational contexts*. World Bank.
- Zhou, Junxiong et al. (2024). “Changes in the Yield Effect of the Preceding Crop in the US Corn Belt Under a Warming Climate”. In: *Global Change Biology* 30.11. e17556 GCB-24-2599, e17556. DOI: <https://doi.org/10.1111/gcb.17556>. eprint: <https://onlinelibrary.wiley.com/doi/pdf/10.1111/gcb.17556>. URL: <https://onlinelibrary.wiley.com/doi/abs/10.1111/gcb.17556>.
- Zrnica, Tijana (2024). “A Note on the Prediction-Powered Bootstrap”. In: *arXiv preprint arXiv:2405.18379*.

Appendix A Superpopulation-based versus design-based inference

This paper focuses on settings where both the ground truth data and the data from the remote sensing map are assumed to be drawn from some superpopulation. This inference framework is in contrast to the design-based inference framework (Särndal et al., 2003) that is commonly used in the remote sensing area estimation literature (Olofsson et al., 2014; Stehman, 2000), where the observed samples from the map data are presumed to constitute the entire population of interest.

We focus on superpopulation-based inference approaches as opposed to design-based inference approaches for three reasons. First, it is common in remote sensing studies to downsample the data from a remote sensing map to save computational resources, especially when the goal is to fit a complex, computationally expensive regression model. For example, (Zhou et al., 2024) downsamples a crop type and crop yield map to fit a model relating crop rotation to crop yield for computational reasons (they find little change in their results across 20 different random downsamplings of the map products). Second, the PPI literature has thus far only developed methods that are theoretically justified in superpopulation-based inference settings. This is not a fundamental limitation of the PPI framework, and future work can extend PPI to design-based inference settings. Third, in our motivating applications N is large, so the variances of the component PPI estimators $\hat{\beta}_{\text{calib}}$, $\hat{\gamma}_{\text{calib}}$, and $\hat{\gamma}_{\text{map}}$ will be similar whether or not one uses a design-based inference or a superpopulation-based inference framework (e.g. in design-based inference $\hat{\gamma}_{\text{map}}$ is viewed as a constant with 0 variance whereas in superpopulation-based inference $\hat{\gamma}_{\text{map}}$ has small variance due to the large sample size N). As a result, we expect that both frameworks will yield confidence intervals of similar widths, with the design-based inference confidence intervals being slightly smaller and the differences diminishing as $N \rightarrow \infty$.

Appendix B Formulas for variance and tuning matrix of $\hat{\beta}_{\text{PPI}}$

In this appendix, we present formulas for the covariance matrix of the proposed estimator $\hat{\beta}_{\text{PPI}}$ and its optimal tuning matrix. We focus on providing explicit formulas in the case of linear regression and logistic regression. The resulting formulas can be found in (Y.-H. Chen and H. Chen, 2000), but for ease of exposition, we provide a slightly different derivation and more explicit expressions in our cases of interest. More formal derivations in a more general setting can be found in the appendix of (Kluger et al., 2025).

Recall that $\hat{\gamma}_{\text{map}}$, $\hat{\beta}_{\text{calib}}$, and $\hat{\gamma}_{\text{calib}}$ are regression coefficient estimates from a generalized linear model (GLM), which could be a linear model or logistic regression model. Moreover, $\hat{\gamma}_{\text{map}}$ is estimated using all N samples $(\hat{X}'_i, \hat{Y}'_i)_{i=1}^N$ of the map-based predictions. Meanwhile $\hat{\beta}_{\text{calib}}$ and $\hat{\gamma}_{\text{calib}}$ are estimated using a uniform random subsample of size n , which is a fraction $\rho = n/N$ of the N samples. $\hat{\beta}_{\text{calib}}$ is estimated using ground truth points $(X_i, Y_i)_{i=1}^n$ and $\hat{\gamma}_{\text{calib}}$ is estimated using the corresponding proxies $(\hat{X}_i, \hat{Y}_i)_{i=1}^n$. For convenience we let (X, Y) denote a random vector with the same distribution as (X_i, Y_i) and (\hat{X}, \hat{Y}) denote a random vector with the same distribution as the map-based predictions (\hat{X}_i, \hat{Y}_i) or (\hat{X}'_i, \hat{Y}'_i) .

Now let $\psi : \mathbb{R} \rightarrow \mathbb{R}$ be a function that specifies the type of GLM being run: $\psi(s) = \frac{1}{2}s^2$ for linear regression and $\psi(s) = \log(1 + e^s)$ for logistic regression with a canonical link function. Note since $\hat{\beta}_{\text{calib}}$ is a regression coefficient from a GLM, it estimates the well-defined quantity

$$\beta_* = \arg \min_{\beta \in \mathbb{R}^p} \mathbb{E}[-Y\beta^\top X + \psi(\beta^\top X)].$$

Similarly, $\hat{\gamma}_{\text{calib}}$ and $\hat{\gamma}_{\text{map}}$ estimate the well defined quantity

$$\gamma_* = \arg \min_{\beta \in \mathbb{R}^p} \mathbb{E}[-\hat{Y}\beta^\top \hat{X} + \psi(\beta^\top \hat{X})].$$

Based on asymptotic theory for M-estimators (e.g., Chapter 5 of (Vaart, 1998)) and since GLM estimators are M-estimators, under standard regularity conditions the 3 component estimators of $\hat{\beta}_{\text{PPI}}$ are asymptotically multivariate normal with

$$\begin{bmatrix} \hat{\beta}_{\text{calib}} \\ \hat{\gamma}_{\text{calib}} \\ \hat{\gamma}_{\text{map}} \end{bmatrix} \sim \mathcal{N} \left(\begin{bmatrix} \beta_* \\ \gamma_* \\ \gamma_* \end{bmatrix}, \frac{1}{n} \begin{bmatrix} D_\beta^{-1} C_{11} D_\beta^{-1} & D_\beta^{-1} C_{12} D_\gamma^{-1} & \rho D_\beta^{-1} C_{12} D_\gamma^{-1} \\ D_\gamma^{-1} C_{12}^\top D_\beta^{-1} & D_\gamma^{-1} C_{22} D_\gamma^{-1} & \rho D_\gamma^{-1} C_{22} D_\gamma^{-1} \\ \rho D_\gamma^{-1} C_{12}^\top D_\beta^{-1} & \rho D_\gamma^{-1} C_{22} D_\gamma^{-1} & \rho D_\gamma^{-1} C_{22} D_\gamma^{-1} \end{bmatrix} \right).$$

Above \sim means approximately distributed as, $\mathcal{N}(\mu, \Sigma)$ denotes a multivariate normal distribution with mean vector μ and covariance matrix Σ , and the component matrices are given by

$$\begin{aligned} D_\beta &= \mathbb{E}[\ddot{\psi}(\beta_*^\top X) X X^\top], \quad D_\gamma = \mathbb{E}[\ddot{\psi}(\gamma_*^\top \hat{X}) \hat{X} \hat{X}^\top], \quad C_{11} = \mathbb{E}[(Y - \dot{\psi}(\beta_*^\top X))^2 X X^\top] \\ C_{12} &= \mathbb{E}[(Y - \dot{\psi}(\beta_*^\top X))(\hat{Y} - \dot{\psi}(\gamma_*^\top \hat{X})) X \hat{X}^\top] \quad \text{and} \quad C_{22} = \mathbb{E}[(\hat{Y} - \dot{\psi}(\gamma_*^\top \hat{X}))^2 \hat{X} \hat{X}^\top], \end{aligned}$$

where $\dot{\psi}(\cdot)$ and $\ddot{\psi}(\cdot)$ give the first and second derivatives of the GLM class-specific function ψ . Now recall $\hat{\beta}_{\text{PPI}}$ takes the form

$$\hat{\beta}_{\text{PPI}, \Omega} = \Omega \hat{\gamma}_{\text{map}} + (\hat{\beta}_{\text{calib}} - \Omega \hat{\gamma}_{\text{calib}}),$$

where $\Omega \in \mathbb{R}^{p \times p}$ is some tuning matrix. Note that by the previous asymptotic normality approximation and the formula for the distribution of a linear transformation of a multivariate Gaussian (i.e., using the fact that $AZ \sim \mathcal{N}(A\mu, A\Sigma A^\top)$ when A is a fixed matrix and $Z \sim \mathcal{N}(\mu, \Sigma)$),

$$\hat{\beta}_{\text{PPI}, \Omega} = \begin{bmatrix} I_{p \times p} & -\Omega & \Omega \end{bmatrix} \begin{bmatrix} \hat{\beta}_{\text{calib}} \\ \hat{\gamma}_{\text{calib}} \\ \hat{\gamma}_{\text{map}} \end{bmatrix} \sim \mathcal{N} \left(\beta_*, \frac{1}{n} V(\Omega) \right),$$

where

$$V(\Omega) = D_\beta^{-1} C_{11} D_\beta^{-1} - (1 - \rho) \Omega [D_\beta^{-1} C_{12} D_\gamma^{-1}]^\top - (1 - \rho) D_\beta^{-1} C_{12} D_\gamma^{-1} \Omega^\top + (1 - \rho) \Omega D_\gamma^{-1} C_{22} D_\gamma^{-1} \Omega^\top.$$

Note that the asymptotic variance of each component of $\hat{\beta}_{\text{PPI}}$ is minimized when the diagonal entries of $V(\Omega)$ are minimized. Since $V(\Omega)$ is quadratic in Ω with the j th diagonal entry only depending on the j th row of Ω , an exercise in linear algebra and multivariate calculus for quadratic functions shows that choosing

$$\Omega_* = D_\beta^{-1} C_{12} C_{22}^{-1} D_\gamma,$$

simultaneously minimizes each diagonal component of $V(\Omega)$. Thus Ω_* is the optimal tuning matrix, and note that it is identical to the tuning matrix used in Equation (4) of (Y.-H. Chen and H. Chen, 2000). Further note that

$$V(\Omega_*) = D_\beta^{-1} C_{11} D_\beta^{-1} - (1 - \rho) D_\beta^{-1} C_{12} C_{22}^{-1} C_{12}^\top D_\beta^{-1},$$

which matches the asymptotic variance found in Equation (5) of (Y.-H. Chen and H. Chen, 2000).

If \hat{D}_β , \hat{D}_γ , \hat{C}_{11} , \hat{C}_{12} and \hat{C}_{22} are data-based estimates of previously defined matrices that converge in probability to D_β , D_γ , C_{11} , C_{12} , and C_{22} , respectively, then choosing the tuning matrix

$$\hat{\Omega} = \hat{D}_\beta^{-1} \hat{C}_{12} \hat{C}_{22}^{-1} \hat{D}_\gamma \quad (2)$$

will be asymptotically optimal. In such settings $\hat{\Omega}$ will converge in probability to Ω_* and asymptotically, $\hat{\beta}_{\text{PPI}}$ will approximately follow a $\mathcal{N}(\beta_*, \frac{1}{n} V(\Omega_*))$ distribution, in which case one can use an approximated covariance matrix for $\hat{\beta}_{\text{PPI}}$ given by

$$\hat{V}_{\text{PPI}} = \frac{1}{n} \left(\hat{D}_\beta^{-1} \hat{C}_{11} \hat{D}_\beta^{-1} - \left(1 - \frac{n}{N}\right) \hat{D}_\beta^{-1} \hat{C}_{12} \hat{C}_{22}^{-1} \hat{C}_{12}^\top \hat{D}_\beta^{-1} \right) \quad (3)$$

and the normal approximation to calculate standard errors and confidence intervals for $\hat{\beta}_{\text{PPI}}$. Note that in this paper we use a bootstrap approach to constructing confidence intervals because it can generalize to other settings without having to find an explicit formula for \hat{V}_{PPI} .

B.1 Explicit formulas in linear regression settings

In linear regression settings $\psi(s) = \frac{1}{2}s^2$, so $\dot{\psi}(s) = s$ and $\ddot{\psi}(s) = 1$. Hence $D_\beta = \mathbb{E}[XX^\top]$, $D_\gamma = \mathbb{E}[\hat{X}\hat{X}^\top]$,

$$C_{11} = \mathbb{E}[(Y - \beta_*^\top X)^2 XX^\top], C_{12} = \mathbb{E}[(Y - \beta_*^\top X)(\hat{Y} - \gamma_*^\top \hat{X})X\hat{X}^\top], \quad \text{and} \quad C_{22} = \mathbb{E}[(\hat{Y} - \gamma_*^\top \hat{X})^2 \hat{X}\hat{X}^\top].$$

Thus one can use the plug in estimators

$$\begin{aligned} \hat{D}_\beta &= \frac{1}{n} \sum_{i=1}^n X_i X_i^\top, \quad \hat{D}_\gamma = \frac{1}{n} \sum_{i=1}^n \hat{X}_i \hat{X}_i^\top, \quad \hat{C}_{11} = \frac{1}{n} \sum_{i=1}^n (Y_i - \hat{\beta}_{\text{calib}}^\top X_i)^2 X_i X_i^\top, \\ \hat{C}_{12} &= \frac{1}{n} \sum_{i=1}^n (Y_i - \hat{\beta}_{\text{calib}}^\top X_i)(\hat{Y}_i - \hat{\gamma}_{\text{calib}}^\top \hat{X}_i) X_i \hat{X}_i^\top, \quad \text{and} \quad \hat{C}_{22} = \frac{1}{n} \sum_{i=1}^n (\hat{Y}_i - \hat{\gamma}_{\text{calib}}^\top \hat{X}_i)^2 \hat{X}_i \hat{X}_i^\top. \end{aligned}$$

One can then plug the above formulas into Equation (2) to obtain an asymptotically optimal tuning matrix choice. They can further plug these formulas into Equation (3) to estimate the variance of $\hat{\beta}_{\text{PPI}}$ with this tuning matrix choice (the estimated variance matrix of $\hat{\beta}_{\text{PPI}}$ can then be used to calculate standard errors and confidence intervals).

B.2 Explicit formulas in logistic regression settings

In logistic regression settings $\psi(s) = \log(1 + e^s)$, so $\dot{\psi}(s) = 1/(1 + e^{-s})$ and $\ddot{\psi}(s) = e^s/(1 + e^s)^2$. We can then similarly use the plug in estimators for D_β , D_γ , C_{11} , C_{22} , and C_{12} given by

$$\begin{aligned} \hat{D}_\beta &= \frac{1}{n} \sum_{i=1}^n \frac{\exp(\hat{\beta}_{\text{calib}}^\top X_i)}{(1 + \exp(\hat{\beta}_{\text{calib}}^\top X_i))^2} X_i X_i^\top, \quad \hat{D}_\gamma = \frac{1}{n} \sum_{i=1}^n \frac{\exp(\hat{\gamma}_{\text{calib}}^\top \hat{X}_i)}{(1 + \exp(\hat{\gamma}_{\text{calib}}^\top \hat{X}_i))^2} \hat{X}_i \hat{X}_i^\top, \\ \hat{C}_{11} &= \frac{1}{n} \sum_{i=1}^n \left(Y_i - \frac{1}{1 + \exp(-\hat{\beta}_{\text{calib}}^\top X_i)} \right)^2 X_i X_i^\top, \quad \hat{C}_{22} = \frac{1}{n} \sum_{i=1}^n \left(\hat{Y}_i - \frac{1}{1 + \exp(-\hat{\gamma}_{\text{calib}}^\top \hat{X}_i)} \right)^2 \hat{X}_i \hat{X}_i^\top \end{aligned}$$

$$\text{and } \hat{C}_{12} = \frac{1}{n} \sum_{i=1}^n \left(Y_i - \frac{1}{1 + \exp(-\hat{\beta}_{\text{calib}}^\top X_i)} \right) \left(\hat{Y}_i - \frac{1}{1 + \exp(-\hat{\gamma}_{\text{calib}}^\top \hat{X}_i)} \right) X_i \hat{X}_i^\top.$$

One can then plug the above formulas into Equation (2) to obtain an asymptotically optimal tuning matrix choice. They can further plug these formulas into Equation (3) to estimate the variance of $\hat{\beta}_{\text{PPI}}$ with this tuning matrix choice (the estimated variance matrix of $\hat{\beta}_{\text{PPI}}$ can then be used to calculate standard errors and confidence intervals).

Appendix C Datasets

We describe the datasets used in the four examples in the paper.

C.1 Example 1: Deforestation logistic regression

For the deforestation response variable, we use $N = 963548$ map product pixels sampled uniformly at random from the NASA Global Forest Cover Change (GFCC) map (Townshend, 2016) (at 30 m resolution) in the study area. The GFCC product is derived from Landsat 5 and Landsat 7 surface reflectance imagery, and includes maps for tree cover percentage in each pixel in five-year increments from 2000 to 2015.

For ground truth, we use a Amazon deforestation and forest disturbance dataset created by (Bullock et al., 2020) using time-series analysis of Landsat imagery and high-resolution imagery from Google Earth between 1995 and 2017. The dataset records the years corresponding to deforestation, degradation, and natural disturbance events at each ground truth point. We use this to construct a binary ground truth dataset restricted to Brazil, in which we consider a point deforested if it experienced a deforestation event between 2000 and 2015. The original dataset is obtained by stratified random sampling, using a stratification map (also created by (Bullock et al., 2020)) that contains 7 strata related to deforestation status. For our experiments, we construct a “uniformly random sampled” ground truth dataset of size $n = 1386$ by downsampling the points in each of the strata to match its area proportion. Using the ground truth dataset, we find that for the “deforested” class, the remotely sensed map has 69% producer’s accuracy and 71% user’s accuracy.

Binarizing the NASA GFCC map product for deforestation. The ground truth points from (Bullock et al., 2020) have binary deforestation values ($Y = 1$ if deforested and $Y = 0$ if not deforested between 2000-2015), while the NASA GFCC map product gives canopy cover percentages over time at each pixel. In order to binarize the continuous map product data, we classify a map pixel as “deforested” if its canopy cover percentage satisfies $\text{canopy}_{2015} - \text{canopy}_{2000} \leq -25\%$. We choose the -25% threshold by visually comparing the map-derived canopy cover change distributions for deforested and non-deforested ground truth points (Figure 6). Most of the deforested ground truth points have a map canopy cover decrease of more than 25%, while most of the non-deforested ground truth points have either a map canopy cover increase, no map canopy cover change, or a map canopy cover decrease of less than 25%.

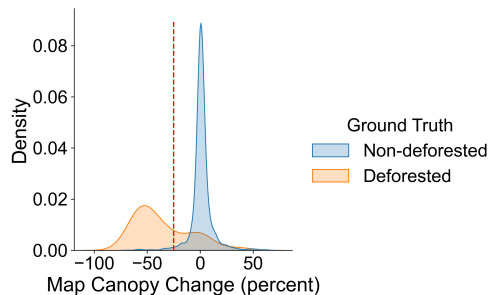


Figure 6: **NASA GFCC map canopy cover change (2000-2015) distributions for non-deforested and deforested ground truth** over $n = 1386$ uniformly random sampled points. The distributions are visualized using kernel density estimation. We choose a -25% deforestation threshold (shown in red) to binarize the map product.

For the covariates, we use a map of Brazilian federal roads in 2000 (Castro Victoria et al., 2021) and the WWF HydroSHEDS Free Flowing Rivers Network map (Grill et al., 2019) (we include all rivers of order at most 3) to compute the distance from each data point to the nearest major road and major river. We obtain elevation and slope from the NASA Digital Elevation Model (NASA Jet Propulsion Laboratory, 2020) at 30 m resolution. Prior work has shown that deforestation in the Brazilian Amazon is more likely to occur near major roads and navigable rivers due to human settlement and economic activities along these transportation networks (Kirby et al., 2006; Laurance et al., 2002; Rosa et al., 2013). Elevation and slope

have been associated with forest cover change; for example, deforestation is generally less likely on sloped terrain (Sandel and Svenning, 2013). Studies have also regressed remotely sensed deforestation against other covariates such as climate, soil fertility, population, and protected area status (Etter et al., 2006; Laurance et al., 2002). Additionally, there exist unofficial, non government built roads in Brazil that are not identified in the federal roads map but may be associated with deforestation (Arima et al., 2016; Brandão Jr and Souza Jr, 2006; Perz et al., 2007; Valle et al., 2024). However, in this paper, we do not use a comprehensive list of covariates that could influence deforestation, because the primary purpose of this regression is to illustrate the methods rather than explain deforestation.

C.2 Example 2: Tree cover linear regression

For the tree cover response variable, we use $N = 983238$ map product points sampled uniformly at random from the 2021 USFS Tree Canopy Cover (TCC) product (USDA Forest Service, 2023) at 30 m resolution. The TCC product is derived from Landsat and Sentinel-2 top-of-atmosphere reflectance data, USDA NASS CDL data, and terrain data. Its tree cover percentage predictions are obtained from random forest models trained on reference data from human-labeled high-resolution imagery. For ground truth, we manually label $n = 983$ high-resolution satellite images from Google Maps for tree cover percentage, by visually estimating the proportion of the 30 m by 30 m image that is covered by trees. The image locations were sampled uniformly at random from the study area. The R^2 coefficient between the remotely sensed and ground truth tree cover percentage values is 0.68.

For the covariates, we use a map of the average Global Aridity Index from 1970-2000 (at 30 arc-seconds resolution) (Trabucco, 2019) and the NASA Digital Elevation Model (NASA Jet Propulsion Laboratory, 2020) (at 30 m resolution). The aridity index is defined as a ratio between precipitation and evapo-transpiration, and is *lower* for more arid areas; its value ranges from 0.02 to 6.55 in our dataset. Increased aridity is associated with lower tree cover (and decreased vegetation in general) (Bastin et al., 2017; Berdugo et al., 2020; Williams et al., 2010). Elevation and slope have also been associated with tree cover globally; there is generally more tree cover at lower elevations (e.g., due to higher temperatures) (Mayor et al., 2017) and on sloped terrain (Sandel and Svenning, 2013). We do not include a comprehensive list of covariates that could influence tree cover, because the primary purpose of this regression is to illustrate uncertainty quantification rather than explain tree cover.

C.3 Example 3: Housing price linear regression

For all variables, we use the MOSAIKS dataset (Rolf et al., 2021) which contains a population-weighted random sample of points in the United States at roughly 1 km resolution. The dataset contains ground truth values across seven variables, as well as corresponding remotely sensed predictions obtained from a machine learning model trained on a subset of the ground truth points. The model runs ridge regression on featurized representations of Google Static Maps satellite imagery. The MOSAIKS predictions generally capture the variables well, with R^2 ranging from 0.45 to 0.91 to depending on the variable. We note that (Proctor et al., 2023) also runs regressions on the MOSAIKS dataset using the ground truth and remotely sensed predictions, but unlike PPI, their coefficient estimation method relies on Bayesian modelling assumptions and does not provide frequentest statistical guarantees for e.g., 95% coverage of the true coefficients.

The ground truth datasets are described in detail in the Supplementary Materials of (Rolf et al., 2021). Housing price per square foot for sales since 2010 are obtained using the Zillow Transaction and Assessment Dataset. Median household income at the census block group level is obtained from the 2015 American Community Survey. Nighttime light intensity is obtained from average radiance values from the 2015 Visible Infrared Imaging Radiometer Suite (VIIRS). Total road length in each ~ 1 km grid cell is computed from the United States Geological Survey National Transportation Dataset.

After removing points with missing variables, there are $N = 46418$ points that have both ground truth and remotely sensed values for housing price (log dollars per square foot), household income (dollars), nighttime light intensity ($\log(1+nW/\text{cm}^2/\text{sr})$), and road length (km). The R^2 coefficient between MOSAIKS predictions and ground truth is 0.85 for nightlights and 0.52 for road length.

For housing price and income, we use the ground truth values for all 46418 points. For nightlights and road length, we take a uniform random subsample of $n = 500$ points as the ground truth calibration set (and

use remotely sensed values for the remaining points). For the GT-only method, we use only the $n = 500$ ground truth points for all four variables. We also compare the regression coefficient point estimates from our methods against the “true coefficients” computed by running linear regression on the full set of 46418 ground truth points for all four variables.

C.4 Example 4: Forest cover linear regression

Similar to the previous example, we use the MOSAIKS dataset (Rolf et al., 2021). The dataset also provides a uniformly-weighted random sample of points in the United States at ~ 1 km resolution. After removing points with missing variables, there are $N = 67968$ points that have both ground truth and remotely sensed values for forest cover percentage, elevation (km), and population ($\log(1 + \text{people})/\text{km}^2$).

The ground truth datasets are described in detail in the Supplementary Materials of (Rolf et al., 2021). Forest cover percentage is obtained from the 2010 Hansen Global Forest Change maps (Hansen et al., 2013), which are derived from Landsat imagery. Elevation is obtained from Mapzen terrain tiles with data from NASA Jet Propulsion Laboratory’s Shuttle Radar Topography Mission. Population density is obtained from the Gridded Population of the World dataset, which uses the 2010 US Population and Housing Census.

As in the previous example, the $N = 67968$ remotely sensed predictions were obtained by (Rolf et al., 2021) using the MOSAIKS prediction model, which runs ridge regression on featurized representations of Google Static Maps satellite imagery. The R^2 coefficient between the MOSAIKS predictions and ground truth is 0.91 for forest cover and 0.73 for population.

For elevation, we use the ground truth values for all 67968 points. For forest cover and population, we take a uniform random subsample of $n = 500$ points as the ground truth calibration set (and use remotely sensed values for the remaining points). For the GT-only method, we use only the $n = 500$ ground truth points for all three variables. We also compare the regression coefficient point estimates from our methods against the “true coefficients” computed by running linear regression on the full set of 67968 ground truth points for all four variables.

To generate the histogram in the right panel of Figure 2 of the main text, we compute PPI and GT-only coefficient estimates using 100 different uniform random subsamples of $n = 500$ ground truth points from the full set of 67968 ground truth points. We use the same set of $N = 67968$ map product points in all 100 trials. Note that the map-only estimate remains the same in all trials.

Appendix D PPI for mean estimation

In this appendix, we describe how to use PPI to estimate the mean value of a remotely sensed variable. We describe ground truth-only, map-only, and PPI estimators. (Note that **area estimation** can be formulated as estimating the mean of a binary variable representing a land use/land cover class. See Appendix E for examples applying PPI for area estimation on remote sensing datasets.)

Ground truth-only estimator. First, **ground truth-only (GT-only)** uncertainty quantification uses ground truth observations, sampled uniformly at random, to estimate the quantity of interest. For example, suppose there is a response variable Y that can be observed over a given area, and we wish to generate a 95% confidence interval for its population mean $\theta^* = E[Y]$. If we have n ground truth observations Y_1, Y_2, \dots, Y_n sampled uniformly at random, we can compute the sample mean

$$\hat{\theta} = \frac{1}{n} \sum_{i=1}^n Y_i, \quad \text{which has standard deviation} \quad \sigma_{\hat{\theta}} = \sqrt{\frac{1}{n} \text{Var}(Y_i)},$$

and estimate the standard deviation with

$$\hat{\sigma}_{\hat{\theta}} = \frac{1}{n} \sqrt{\sum_{i=1}^n (Y_i - \hat{\theta})^2}$$

to produce the GT-only 95% confidence interval

$$C = (\hat{\theta} - 1.96 \cdot \hat{\sigma}_{\hat{\theta}}, \hat{\theta} + 1.96 \cdot \hat{\sigma}_{\hat{\theta}}).$$

If the size n of the ground truth dataset is small, which is often the case in environmental applications, the GT-only confidence interval will be large.

Map-only estimator: Use only the remote sensing map. If we have a remote sensing data product with a large number N of predictions $\hat{Y}_1, \hat{Y}_2, \dots, \hat{Y}_N$ over the area of interest, we could treat these predictions like ground truth points and use the formula above with \hat{Y} in place of Y . This would produce a much smaller confidence interval, since we would use $N \gg n$ in the denominator of the standard error. However, this **map-only estimator** approach may result in a biased estimate, and the confidence interval is not guaranteed to have a 95% coverage rate of the true parameter of interest. This is because the map-only estimator does not account for error or uncertainty in the model used to generate the map product predictions.

Prediction-Powered Inference: Map + ground truth. PPI (Angelopoulos et al., 2023b) evaluates the accuracy of the map product by comparing the ground truth labels Y_1, Y_2, \dots, Y_n to the map product predictions $\hat{Y}_1, \hat{Y}_2, \dots, \hat{Y}_n$ at the corresponding ground truth point locations. This **calibration set** of n points is a simple or stratified random sample over the region of interest, and it must be separate from the training dataset used to train the machine learning model. PPI uses the calibration set to correct for bias in the map-only estimate computed from the N unlabeled map points $\hat{Y}'_1, \hat{Y}'_2, \dots, \hat{Y}'_N$.

For a concrete example, suppose we wish to estimate $\theta^* = E[Y]$ as before. In the special case of estimating $\theta^* = E[Y]$, the PPI point estimate is

$$\hat{\theta}_{\text{PPI}} = \underbrace{\frac{1}{N} \sum_{i=1}^N \hat{Y}'_i}_{\text{map-only estimate}} - \underbrace{\frac{1}{n} \sum_{i=1}^n (\hat{Y}_i - Y_i)}_{\text{bias correction}},$$

which coincides precisely with an estimator previously studied in the remote sensing literature (see Equation 4c of (McRoberts et al., 2022)). Assuming the map sample and calibration sample are independent, the

standard deviation of this estimator is

$$\begin{aligned}\sigma_{\text{PPI}} &= \sqrt{\frac{1}{N}\text{Var}(\hat{Y}'_i) + \frac{1}{n}\text{Var}(\hat{Y}_i - Y_i)} \\ &\approx \sqrt{\frac{1}{n}\text{Var}(\hat{Y}_i - Y_i)},\end{aligned}$$

where the approximation holds when N is much larger than n . Letting $\hat{\sigma}_{\text{PPI}}$ be an estimate of σ_{PPI} based on plugging sample variance estimates into the formula for σ_{PPI} , the PPI 95% confidence interval is given by

$$C_{\text{PPI}} = (\hat{\theta}_{\text{PPI}} - 1.96 \cdot \hat{\sigma}_{\text{PPI}}, \hat{\theta}_{\text{PPI}} + 1.96 \cdot \hat{\sigma}_{\text{PPI}}).$$

The first term in σ_{PPI} is the variance corresponding to using only map predictions to estimate θ , i.e. $\frac{1}{N}\text{Var}(\hat{Y}'_i)$. The second term is the variance from the bias correction, $\frac{1}{n}\text{Var}(\hat{Y}_i - Y_i)$. As the number of map product points N grows large, σ_{PPI} approaches $\sqrt{\frac{1}{n}\text{Var}(\hat{Y}_i - Y_i)}$. This will be a realistic approximation in many cases, since remote sensing maps at a global, national, or province level can contain millions or even billions of pixels, whereas the number of ground truth points n is commonly in the hundreds or thousands. The greater the accuracy of the map product, the smaller $\text{Var}(\hat{Y}_i - Y_i)$ will be and the smaller the PPI confidence interval will be. Note that the PPI confidence interval is smaller than the GT-only confidence interval if $\text{Var}(\hat{Y}_i - Y_i) < \text{Var}(Y_i)$.

Like PPI, the post-stratified area estimator combines a map product with a small amount of ground truth data to make a precise and unbiased estimate. The post-stratified estimator and PPI produce similar outputs for area estimation; for more detailed comparisons of the two methods, see Appendices E and F. However, the post-stratified estimator only applies to area estimation, not regression coefficient estimation, while PPI can be applied to both (Figure 1 in the main text). Similarly, an estimator from (McRoberts et al., 2022) coincides precisely with the PPI estimator in the context of mean estimation, but does not apply to the setting of regression coefficient estimation.

Appendix E Area estimation experiments

In this appendix, we apply PPI and other methods to **area estimation** tasks with both ground truth and remotely sensed data.

We first describe two well-known methods for area estimation (stratified estimator and post-stratified estimator). These methods were introduced in (Cochran, 1977) and are commonly used in the remote sensing community (Olofsson et al., 2013, 2014). PPI for area estimation (described in Appendix D) produces similar confidence intervals as the post-stratified estimator; for a mathematical comparison, see Appendix F.

Then, we apply PPI, the stratified estimator, and the post-stratified estimator to two area estimation use cases (Iowa maize crop area and Brazilian Amazon deforestation area). We also compare results with the GT-only and map-only mean estimation methods described in Appendix D.

E.1 Stratified estimator

Stratified random sampling uses remotely sensed maps to determine a sampling strategy for ground truth points that reduces the variance of estimates. The **stratified estimator** is commonly used in the remote sensing community.

We first use a map product to partition the area of interest into K strata (sub-areas) such that the response variable is predicted to have low variance within each stratum. Then we sample n_k ground truth points uniformly at random from each stratum $1 \leq k \leq K$. We can choose n_k to be larger for strata predicted to have higher uncertainty to decrease the standard error within the strata and hence make the overall standard error smaller with the same total number of sample units.

Suppose we observe the response variable Y over a given area, and we wish to estimate $\theta^* = E[Y]$ using a stratified random sample. For each stratum k , we compute the stratum sample mean $\hat{\theta}_k$ and stratum standard error $\hat{\sigma}_k$ using the same formulae as the GT-only method from Appendix D. Suppose that in the map product, each stratum k takes up proportion $0 < A_k < 1$ of the total area (with $\sum_{k=1}^K A_k = 1$). Then, we compute the stratified mean

$$\hat{\theta}_{\text{strat}} = \sum_{k=1}^K A_k \hat{\theta}_k$$

and stratified standard error

$$\hat{\sigma}_{\text{strat}} = \sqrt{\sum_{k=1}^K A_k^2 \cdot \hat{\sigma}_k^2}$$

to produce the stratified 95% confidence interval

$$C_{\text{strat}} = (\hat{\theta}_{\text{strat}} - 1.96 \cdot \hat{\sigma}_{\text{strat}}, \hat{\theta}_{\text{strat}} + 1.96 \cdot \hat{\sigma}_{\text{strat}}).$$

The advantage of stratified estimation with an accurate map and well-chosen sampling strategy is that the variance within each stratum will be small, which results in a smaller overall confidence interval compared to the GT-only method. If the map predictions are inaccurate, then the ground truth points likely have higher variance within each map stratum, resulting in a larger confidence interval. Thus the uncertainty quantification incorporates the accuracy of the map product predictions.

For example, in our Brazilian Amazon deforestation area estimation use case, we use a remotely sensed stratification map created by (Bullock et al., 2020) using Landsat surface reflectance imagery at 30 m resolution. The map (Figure 7) partitions the Amazon into seven strata related to forest change from 1995-2017: stable forest, stable non-forest, deforestation, natural disturbance, natural disturbance and deforestation, regrowth, and buffer. The strata are designed so that points within each stratum have low variance in deforestation status (for instance, most points in the “stable forest” and “stable non-forest” strata do not experience deforestation in the time period of interest). As a result, our stratified confidence interval for deforestation area is smaller than the GT-only confidence interval.

PPI can be used with either uniform random sampling or stratified random sampling of the ground truth points (Fisch et al., 2024). **Stratified (weighted) PPI** can be applied as follows for mean estimation.

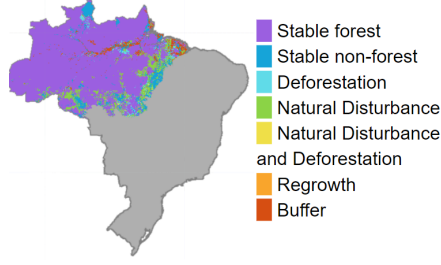


Figure 7: **Stratified estimation is a commonly used approach with remote sensing maps.** This example shows a map of the Brazilian Amazon used for stratification. The strata are designed so that points within each stratum have low variance in deforestation status, which reduces the uncertainty when estimating area deforested. Adapted from (Bullock et al., 2020).

Each ground truth value Y_i and labeled prediction \hat{Y}_i is multiplied by weight $w_i = A_k \frac{n}{n_k}$ where k is the stratum where point i is located, A_k is the area proportion of stratum k , n_k is the number of ground truth sample units in stratum k , and $n = \sum_{k=1}^K n_k$. (Note that the weights are designed such that the sum of weights of all n_k ground truth points in stratum k is $A_k n$, and the sum of weights of all n ground truth points is $\sum_{k=1}^K A_k n = n$. If the points were uniformly randomly sampled, this would be equivalent to only having a single “stratum,” and each point would have weight 1.) Similarly, each unlabeled prediction \hat{Y}'_i in stratum k is multiplied by weight $w_i = A_k \frac{N}{N_k}$ where N_k is the number of map product points in stratum k and $N = \sum_{k=1}^K N_k$. Then the same PPI formulae as in Appendix D can be used.

E.2 Post-stratified area estimator

The **post-stratified area estimator**, commonly used in the remote sensing community, utilizes the confusion matrix between ground truth and map product land cover labels to estimate the area of a land cover class (Card, 1982; Olofsson et al., 2013; Stehman, 2013). Like PPI, the post-stratified area estimator computes confidence intervals by using ground truth points to correct for bias in the map product estimates. This can be viewed as a correction that uses the map errors relative to the ground truth points to modify the map-only area estimates. We show mathematically in Appendix F that PPI and the post-stratified area estimator result in similar confidence intervals as the number of map product points N grows large. However, unlike PPI, the post-stratified area estimator only applies to area estimation but not regression coefficient estimation.

Turning to the method, suppose we have a map product with K land cover classes, as well as n randomly sampled ground truth points. The post-stratified area estimator constructs the $K \times K$ misclassification confusion matrix between ground truth points and map product predictions at the ground truth point locations. For each $1 \leq i \leq K$ and $1 \leq j \leq K$, let n_{ij} denote the number of points that are in map class i and ground truth class j . Also let $n_{i.} = \sum_{j=1}^K n_{ij}$ denote the total number of ground truth samples that have map class i . For each class $1 \leq i \leq K$, let $0 < A_i < 1$ denote the proportion of the total map area taken up by the map class.

Then, motivated by the formula $\mathbb{P}(Y = j) = \sum_{i=1}^K \mathbb{P}(\hat{Y} = i) \cdot \mathbb{P}(Y = j \mid \hat{Y} = i)$, the post-stratified area estimate for the proportion of area of class j is

$$\hat{\theta}_{j,\text{post}} = \sum_{i=1}^K A_i \frac{n_{ij}}{n_{i.}}$$

with corresponding standard error

$$\hat{\sigma}_{j,\text{post}} = \sqrt{\sum_{i=1}^K A_i^2 \frac{\frac{n_{ij}}{n_{i.}} (1 - \frac{n_{ij}}{n_{i.}})}{n_{i.}}}$$

The 95% confidence interval for the proportion of area of class j is

$$C_{j,\text{post}} = (\hat{\theta}_{j,\text{post}} - 1.96 \cdot \hat{\sigma}_{j,\text{post}}, \hat{\theta}_{j,\text{post}} + 1.96 \cdot \hat{\sigma}_{j,\text{post}}).$$

Area estimation is a special case of mean estimation in which we estimate the mean of a binary variable that is 1 for all points in class j and 0 for all points outside of class j . Thus, we can also perform area estimation using methods such as PPI and stratified estimation.

If the n ground truth points are obtained by stratified random sampling using the K map land cover classes as the strata, the post-stratified confidence interval computed using this data is identical to the stratified confidence interval (Olofsson et al., 2013). However, unlike the stratified estimator, the post-stratified estimator can be applied even if the ground truth points are obtained using uniform random sampling.

E.3 Area estimation examples

In this section, we demonstrate uncertainty quantification for two area estimation use cases. First, we simulate estimating maize area in Iowa in 2022, artificially degrading the map product quality relative to simulated “ground truth” points, in order to observe the effect of map product noise and bias on the area estimate under different methods. We will see through this simulation the importance of bias correction before using maps to estimate total area. We then use real ground truth data and real map products developed by researchers to estimate change in tree cover in the Brazilian Amazon in 2000–2015. We compare the GT-only, map-only (pixel-counting), stratified, post-stratified, PPI, and stratified PPI estimators.

In each use case, we use binary data where each point has value 1 if it belongs to the land cover class of interest (e.g., cropland or deforested land), and value 0 otherwise. Then, estimating the area fraction of the land cover class is equivalent to estimating the mean of all points in the region.

We use the PPI-PYTHON software package to implement the unweighted and weighted versions of PPI for our area estimation use cases. The software includes a tuning parameter λ that we set using the map product points and ground-truth points. The confidence intervals are unbiased and guaranteed to have the appropriate (e.g., 95%) coverage of the true area fraction even with this data-driven tuning (Angelopoulos et al., 2023a).

Data and code for these use cases are available at <https://github.com/Earth-Intelligence-Lab/uncertainty-quantification>.

E.3.1 Simulation: Maize area in Iowa

Problem Formulation We simulate estimating the fraction of maize area in Iowa in 2022. To probe the effect of map product noise and bias on different methods, we artificially degrade the map product quality relative to simulated “ground truth” points, as described next.

For this simulation, we use the USDA’s Cropland Data Layer (CDL) (USDA NASS, 2024) as the ground truth for crop types in Iowa. CDL is a crop type land cover map created using satellite imagery and agricultural ground truth data in the continental United States. It has 94.2% producer’s accuracy and 97.2% user’s accuracy for the maize land cover class in Iowa. We sample $N = 100000$ locations uniformly at random from a binary maize/non-maize map derived from CDL (Figure 8). The mean of the 100000 map product points is 0.35, which we will consider the “true” fraction of maize for the simulation.

In each trial, we sample $n = 100$ “ground truth” points uniformly at random from the $N = 100000$ map product points. Initially, we set the map product and ground truth equal to each other at the 100 ground truth locations. We then experiment with degrading the map product quality as follows. We systematically add noise or bias to the map product points while keeping the ground truth points constant, and then compare our maize fraction estimates across the map-only (pixel-counting), GT-only, and PPI estimators. We average results over 100 trials.

Adding unbiased noise. We define adding “unbiased noise” at level p to the map product as resampling each of the 100000 map product points with probability p from the Bernoulli(0.35) distribution. In other words, about p fraction of the points are randomly labeled, while the remaining $1 - p$ points are unchanged. Each resampled point is labeled as maize with probability 0.35 and non-maize with probability 0.65. We experiment with noise probabilities p from 0 to 1 at increments of 0.1.

Adding bias. We also consider adding bias to the map product. Here, we define adding bias p to the map product as resampling each of the 100000 map product points with probability 0.4 from the Bernoulli(p) distribution. In other words, about 40% of the points are randomly labeled, while the remaining 60% points are unchanged. Each resampled point is labeled as maize with probability p and non-maize with probability $1 - p$. We experiment with bias values p from 0 to 1 at increments of 0.1. When $p = 0.35$, this does not add bias, but as p ranges farther from 0.35, the amount of bias increases.

Results As we add increasing amounts of random noise to the map, all confidence intervals for maize area remain centered at the true maize fraction of 0.35 (Figure 9). This is what we expect, since our noise-adding process resamples from the Bernoulli(0.35) distribution, causing the overall fraction of maize to remain the same. The GT-only confidence interval stays constant because it only uses ground truth points. The map-only confidence intervals are small because $N = 100000$ is large, but they do not account for error in the map product. However, the map-only confidence intervals remain unbiased because the map still has true maize fraction close to 0.35 regardless of noise level.

When the noise probability is low, the PPI confidence intervals are significantly smaller than the GT-only intervals. This is because the error of the map product ($\hat{Y} - Y$) is small at the ground truth locations, so the variance of this error is also small, resulting in a small PPI standard error. As noise increases, the variance of the error of the map product increases; the PPI confidence intervals grow wider, eventually converging to the GT-only confidence interval at noise probability $p = 1$. (At $p = 1$, the map is complete noise and therefore does not provide any information for estimating the area beyond the information contained in the ground truth sample.) Consequently, the PPI effective sample size decreases from $n_{\text{effective}} = 578$ when $p = 0.1$ to $n_{\text{effective}} = 100$ when $p = 1$ (which matches the number of actual ground truth points $n = 100$). Thus, the effectiveness of PPI is dependent on the quality of the map product. The post-stratified confidence intervals and effective sample sizes are nearly identical to those of PPI.

The estimated maize fraction confidence intervals after adding bias to the map product are shown in Figure 10. Again, the GT-only confidence interval stays constant and remains centered at the true maize fraction because it only uses the ground truth points. As bias increases, the fraction of map product points labeled as “maize” increases. As a result, the map-only estimates increase with the bias value, and generally do not remain centered at the true maize fraction of 0.35. The map-only confidence intervals are small because $N = 100000$ is large, but they are unreliable because they do not correct for the bias in the map product. In contrast, the PPI estimates remain centered at the true maize fraction because PPI corrects for bias in the map product. The PPI confidence intervals are smaller than the GT-only intervals because the variance of the map product error $\hat{Y} - Y$ is small (since only about 40% of the map product points are resampled, regardless of bias level). Thus, PPI provides unbiased estimates with lower uncertainty than using only the ground truth points. Again, the post-stratified confidence intervals and effective sample sizes are nearly identical to those of PPI, as expected.

We also plot the maize fraction confidence intervals against overall map accuracy for both the noise and bias experiments (Figure 11). As noise increases, map accuracy decreases, so low map accuracy is associated with wide PPI and post-stratified confidence intervals. Thus, the left panel of Figure 11 resembles an inverted version of the left panel of Figure 9.

As bias increases and the fraction of map product points labeled as “maize” increases, map accuracy decreases linearly. (To see this, note that if each resampled point is labeled as maize with probability p , then an expected $0.35(p) + 0.65(1 - p) = 0.65 - 0.3p$ fraction of the resampled points will match the ground

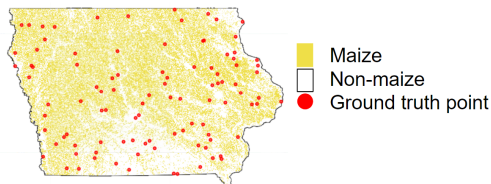


Figure 8: **Iowa maize area estimation datasets.** The Iowa maize binary map product is derived from the USDA’s Cropland Data Layer, and $n = 100$ uniformly randomly sampled “ground truth points” are shown.

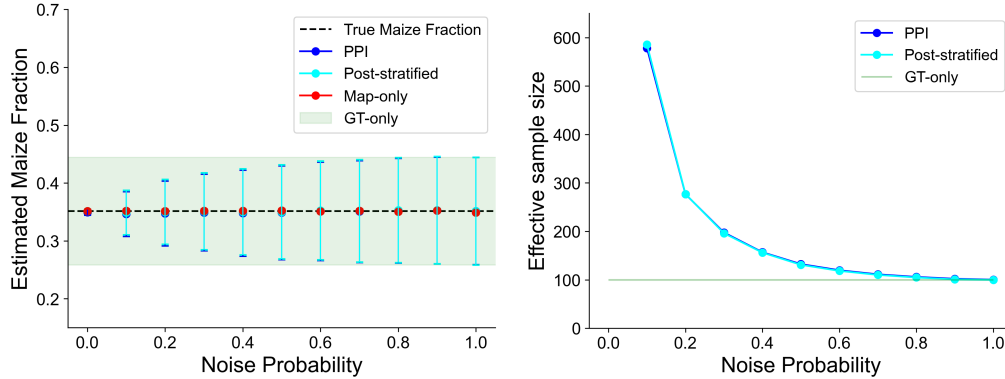


Figure 9: **Simulation estimating maize fraction under different levels of map noise** using $N = 100000$ map product points and $n = 100$ “ground truth” points. Post-stratified and PPI results are overlapping. Left: Maize fraction 95% confidence intervals at different noise levels. Right: Maize fraction effective sample size at different noise levels. (At noise level p , about p fraction of the points are resampled, while the remaining $1 - p$ points are unchanged. Each resampled point is labeled as maize with probability 0.35 (the true maize fraction) and non-maize with probability 0.65.)

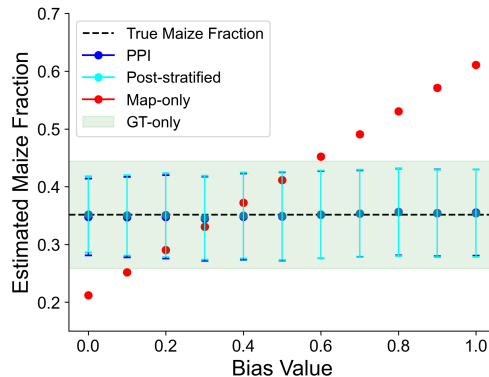


Figure 10: **Simulation estimating maize fraction 95% confidence intervals under different levels of map bias** using $N = 100000$ map product points and $n = 100$ “ground truth” points. Post-stratified and PPI confidence intervals are overlapping. (Noise is fixed at 0.4 so about 40% of the points are resampled. At bias p , each resampled point is labeled as maize with probability p and non-maize with probability $1 - p$.)

truth.) Thus, the map-only estimates of maize fraction decrease linearly as map accuracy increases. In the right panel of Figure 11, a map accuracy of 0.86 corresponds to a map-only maize fraction estimate of 0.21, significantly lower than the true fraction of 0.35. This shows that even a map with high map accuracy can yield biased estimates under the map-only (pixel-counting) estimator.

E.3.2 Deforestation area in Brazilian Amazon

Problem Formulation Next, we move on to real data and estimate the fraction of deforestation in the Brazilian Amazon from 2000 to 2015, comparing confidence interval widths across methods.

We create a binary deforestation map product using all $N = 4.4 \times 10^9$ pixels from the NASA Global Forest Cover Change (GFCC) map (Townshend, 2016) (at 30 m resolution) in the study area (Figure 12). The GFCC product is derived from Landsat 5 and Landsat 7 surface reflectance imagery, and includes maps for tree cover percentage in each pixel in five-year increments from 2000 to 2015. We consider a map pixel deforested if its canopy cover percentage satisfies $\text{canopy}_{2015} - \text{canopy}_{2000} \leq -25\%$ (Figure 6 in Appendix C).

We use a ground truth Amazon deforestation and forest disturbance dataset created by (Bullock et

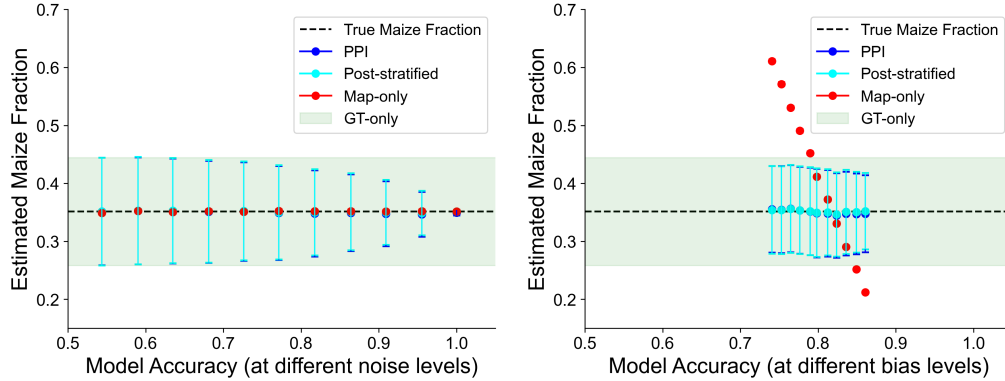


Figure 11: **Simulation estimating maize fraction 95% confidence intervals at different map product overall accuracy levels** obtained by varying noise (left) and bias (right), using $N = 100000$ map product points and $n = 100$ “ground truth” points. Post-stratified and PPI confidence intervals are overlapping.

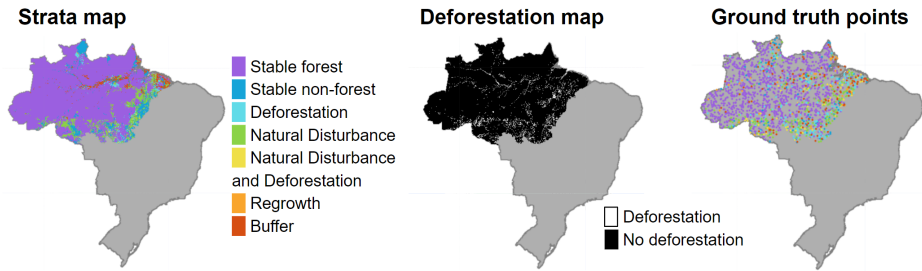


Figure 12: **Brazilian Amazon deforestation area estimation datasets.** Left: Stratification map from (Bullock et al., 2020). Center: Binary map of deforestation from 2000-2015 derived from NASA Global Forest Cover Change. Right: $n = 1386$ ground truth points from (Bullock et al., 2020), colored according to the stratum from which they are sampled.

al., 2020) using time-series analysis of Landsat imagery and high-resolution imagery from Google Earth between 1995 and 2017. The dataset records the years corresponding to deforestation, degradation, and natural disturbance events at each ground truth point. We use this to construct a binary ground truth dataset restricted to Brazil, in which we consider a point deforested if it experienced a deforestation event between 2000 and 2015. The original dataset is obtained by stratified random sampling, using a stratification map (also created by (Bullock et al., 2020)) that contains 7 strata related to deforestation status. To generate a GT-only estimate baseline, we construct a “uniformly random sampled” ground truth dataset by downsampling the points in each of the strata to match its area proportion. For a fair comparison, we also downsample the original stratified ground truth dataset to match the size of the “uniformly random” dataset. This results in two ground truth datasets of $n = 1386$ points each, corresponding to uniform random sampling and stratified random sampling. Both ground truth datasets are used with PPI to obtain confidence intervals.

Results Each method results in a point estimate that between 5% to 6% of the Brazilian Amazon was deforested between 2000 and 2015. The stratified, post-stratified, and PPI estimators all result in smaller 95% confidence intervals for estimated deforestation than GT-only estimation (Figure 13). The post-stratified and PPI confidence intervals are fairly similar, with respective effective sample sizes that are 1.9 and 1.8 times the actual number of ground truth sample points. The stratified and stratified PPI confidence intervals have the best performance, with effective sample sizes that outperform the GT-only method by a factor of about 2.4. (Put differently, stratified PPI has effective sample size 3382, so using the remotely sensed deforestation map added the equivalent of $3382 - 1386 = 1996$ ground truth sample points.) Thus, the methods that use both map product and ground truth reduce uncertainty in our estimates, compared to using only ground

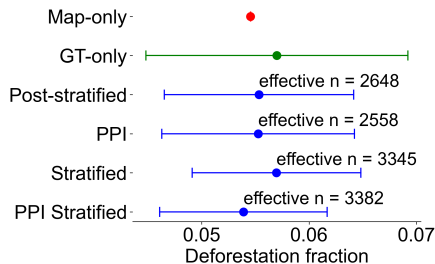


Figure 13: **Brazilian Amazon deforestation 95% confidence intervals** using $N = 4.4 \times 10^9$ map product points and $n = 1386$ ground truth points. The stratified, post-stratified, and PPI estimators all result in smaller confidence intervals for estimated deforestation than GT-only estimation, with the stratified estimator and stratified PPI having the best performances.

truth. In particular, the stratified estimator is effective because the strata map is designed so that points within each stratum have low variance in deforestation status.

In this case, the map-only (pixel-counting) estimate — using only the map to estimate deforestation without any bias correction via ground truth labels — falls within the other confidence intervals, suggesting that the NASA Global Forest Cover Change map has small bias for estimating deforestation area. However, we emphasize that this would not have been clear without the ground truth data, and ground truth data is still necessary to check the reliability of the map product for deforestation analysis.

E.4 Discussion

Bias is the main issue for map-only estimates. Our experiments illustrated that a map-only area estimate from a map without bias correction can yield incorrect inferences, and we differentiated between the influence of noise versus bias. In our simulation estimating maize fraction, map-only estimates deviated from the true maize fraction of 0.35 as the bias of the crop type map increased. Furthermore, map accuracy is not necessarily a good proxy for bias; even at seemingly high map accuracies (accuracy > 0.85), the map-only approach estimated maize fraction at 0.21 (a 40% underestimate).

Stratification vs. Post-stratification vs. PPI. How much stratified, post-stratified, and PPI estimators reduce uncertainty relative to the GT-only estimator depends on the quality of the map product. In stratification, the strata map should be designed such that the variance of the quantity of interest is low within each stratum. In PPI (and the post-stratified method), the variance of the difference between the map product predictions \hat{Y} and the ground truth values Y should be low. In our maize fraction experiments, a highly accurate map (accuracy = 0.96) was equivalent to having nearly $6\times$ as much ground truth data, whereas a low-accuracy map (accuracy = 0.73) only increased the effective sample size by $1.2\times$.

Empirically, when estimating deforestation fraction in the Brazilian Amazon, we observed the smallest confidence intervals when stratification was used alone or in conjunction with PPI. This is a result of well-designed strata based on a remote sensing map of forest disturbance categories. PPI and the post-stratified estimator yielded comparable interval widths to each other. This is expected, as the post-stratified estimator yields similar confidence intervals as PPI when N is large (Appendix F).

An advantage of PPI compared to the stratified estimator is its flexibility. While the stratified estimator requires us to choose a map product before sampling, PPI can be applied to any map product and any randomly sampled ground truth dataset. Given the expensive nature of ground truth data collection, sampling without choosing a strata map and then using PPI to obtain confidence intervals may result in the best performance across a variety of downstream use cases. Or, if stratified samples are already available from area estimation, they can be combined with PPI to estimate regression coefficients.

Appendix F Mathematical comparison of PPI and post-stratified area estimator

We show that when the number of map product points N is large, the PPI and post-stratified area estimator confidence intervals are similar. In particular, we show (1) that they have approximately the same length when the number of sample units is large and (2) they are centered on the same point. These two facts together provide a mathematical explanation for why PPI and the post-stratified estimator approximately agree in all of our experiments.

We begin with notation. Estimating the area proportion of a land cover class in a given region is equivalent to estimating the mean of a binary variable Y , where $Y = 1$ for points in the class and $Y = 0$ for points outside the class. Suppose we have n uniformly random sampled ground truth points Y_1, Y_2, \dots, Y_n and N map product points $\hat{Y}_1, \hat{Y}_2, \dots, \hat{Y}_N$. For all $0 \leq i, j \leq 1$, let n_{ij} denote the number of ground truth points that are in both map class i and ground truth class j . Let $n_{.i} = n_{i0} + n_{i1}$ denote the total number of ground truth points in map class i , and $n_{.i} = n_{0i} + n_{1i}$ denote the total number of ground truth points in ground truth class i . Furthermore, let A_i denote the fraction of the map product that is in class i . We have $A_0 + A_1 = 1$. The map-only area estimate, which we will correct for bias, is A_1 . We will use the approximations $A_0 \approx \frac{n_{0.}}{n}$ and $A_1 \approx \frac{n_{1.}}{n}$. This is a reasonable approximation since the n ground truth locations are sampled uniformly at random.

With this notation, we have the following,

$$\begin{aligned} \sum_{i=1}^n Y_i &= n_{.1} \\ \sum_{i=1}^n \hat{Y}_i &= n_{1.} \\ \text{Var}_n(Y) &= \frac{n_{.0}n_{.1}}{n^2} \\ \text{Var}_N(\hat{Y}) &= A_0A_1 \approx \frac{n_{0.}n_{1.}}{n^2} \text{ and} \\ \text{Cov}_n(Y, \hat{Y}) &= \frac{n_{00}n_{11} - n_{01}n_{10}}{n^2}. \end{aligned}$$

Standard errors. We now turn to the PPI standard error. We have the standard deviation of the tuned PPI estimator from (Angelopoulos et al., 2023a)

$$\begin{aligned} \sigma_{\text{PPI}} &\rightarrow \sqrt{\frac{1}{n} \text{Var}(Y - \lambda \hat{Y})} && \text{since } N \gg n \\ &= \sqrt{\frac{1}{n} \left(\text{Var}(Y) + \lambda^2 \text{Var}(\hat{Y}) - 2\lambda \text{Cov}(Y, \hat{Y}) \right)} && \text{expanding out } \text{Var}(Y - \lambda \hat{Y}) \\ &\rightarrow \sqrt{\frac{1}{n} \left(\text{Var}(Y) - \frac{\text{Cov}(Y, \hat{Y})^2}{\text{Var}(\hat{Y})} \right)} && \text{plugging in } \lambda \\ &\approx \sqrt{\frac{1}{n} \left(\frac{n_{.0}n_{.1}}{n^2} - \frac{(n_{00}n_{11} - n_{01}n_{10})^2}{n^2 n_{0.}n_{1.}} \right)} && \text{plugging in } \text{Var}(Y), \text{Var}(\hat{Y}), \text{Cov}(Y, \hat{Y}) \\ &= \sqrt{\frac{1}{n^2 n_{0.}n_{1.}} (n_{01}n_{00}n_{10} + n_{01}n_{00}n_{11} + n_{11}n_{10}n_{00} + n_{11}n_{10}n_{01})} && \text{using algebraic manipulation.} \end{aligned}$$

Above, we use the fact that as $n, N \rightarrow \infty$, the PPI tuning parameter (from Example 6.1 of (Angelopoulos et al., 2023a)) behaves as

$$\lambda \rightarrow \frac{\text{Cov}_n(Y, \hat{Y})}{\text{Var}_N(\hat{Y})} \approx \frac{n_{00}n_{11} - n_{01}n_{10}}{n_{0.}n_{1.}}.$$

A standard error estimate $\hat{\sigma}_{\text{PPI}}$ of σ_{PPI} also satisfies the above equations.

We compare this with the post-stratified estimator standard error

$$\begin{aligned}
\hat{\sigma}_{\text{post}} &= \sqrt{A_0^2 \frac{n_{00} n_{01}}{n_{0\cdot} n_{0\cdot}} + A_1^2 \frac{n_{10} n_{11}}{n_{1\cdot} n_{1\cdot}}} \\
&\approx \sqrt{\left(\frac{n_{0\cdot}}{n}\right)^2 \times \frac{n_{00} n_{01}}{n_{0\cdot} n_{0\cdot}} + \left(\frac{n_{1\cdot}}{n}\right)^2 \times \frac{n_{10} n_{11}}{n_{1\cdot} n_{1\cdot}}} && \text{plugging in } A_0 \text{ and } A_1 \\
&= \sqrt{\frac{1}{n^2 n_{0\cdot} n_{1\cdot}} (n_{01} n_{00} n_{10} + n_{01} n_{00} n_{11} + n_{11} n_{10} n_{00} + n_{11} n_{10} n_{01})} && \text{using algebraic manipulation.}
\end{aligned}$$

The expressions we arrive at for PPI and the post-stratified estimator agree, indicating that for large sample sizes the standard errors are approximately equal. This implies that the confidence intervals from the two methods will have the same width.

Point estimates. Next, we show that the PPI and post-stratified confidence intervals are centered around the same point. Turning first to the PPI point estimate

$$\begin{aligned}
\hat{\theta}_{\text{PPI}} &= \lambda A_1 - \frac{1}{n} \sum_{i=1}^n (\lambda \hat{Y}_i - Y_i) \\
&\approx \frac{\lambda n_{1\cdot}}{n} - \frac{\lambda n_{1\cdot} - n_{\cdot 1}}{n} && \text{plugging in } A_1, \sum_{i=1}^n Y_i, \text{ and } \sum_{i=1}^n \hat{Y}_i \\
&= \frac{n_{\cdot 1}}{n}
\end{aligned}$$

The post-stratified area point estimate is

$$\begin{aligned}
\hat{\theta}_{\text{post}} &= A_0 \frac{n_{01}}{n_{0\cdot}} + A_1 \frac{n_{11}}{n_{1\cdot}} \\
&\approx \frac{n_{0\cdot}}{n} \times \frac{n_{01}}{n_{0\cdot}} + \frac{n_{1\cdot}}{n} \times \frac{n_{11}}{n_{1\cdot}} && \text{plugging in } A_0 \text{ and } A_1 \\
&= \frac{n_{\cdot 1}}{n}
\end{aligned}$$

We see that the final expressions are equal, which means the point estimates are approximately equal.

Appendix G Simulating mean reversion bias in maps

In Section 4, we simulate adding noise and nonlinear bias to the map products from Example 4 (forest cover linear regression). In this appendix, we simulate another model of map bias: linear mean reversion. Under this type of bias, the map underestimates high ground truth values and overestimates low ground truth values.

Using the same MOSAIKS dataset as Section 4, we simulate different levels of mean reversion bias in the population map (error-in- X), the forest cover map (error-in- Y), or both (error-in-both). The elevation dataset is not altered. We compare the resulting 95% coefficient confidence intervals at different levels of simulated map bias using map-only, GT-only, and PPI methods.

Bias To simulate bias for the ground truth population covariate X_{pop} , we linearly interpolate between X_{pop} and the mean $\mu_{X_{\text{pop}}}$ of all X_{pop} values in the full ground truth dataset (67968 points). The resulting simulated map product value at “bias level c ” is

$$X_{\text{pop}}^{\text{map}} = c\mu_{X_{\text{pop}}} + (1 - c)X_{\text{pop}}.$$

Similarly, for the forest cover response variable Y with mean μ_Y , the simulated map product value at each point is

$$Y^{\text{map}} = c\mu_Y + (1 - c)Y.$$

We experiment with bias levels c from 0 to 0.8 at increments of 0.1. When $c = 0$, the simulated map is the same as the full ground truth map.

Results The coefficient point estimates and 95% confidence intervals at each bias level are shown in Figure 14. We compare results for the map-only, GT-only, and PPI estimators. (For all experiments in this section, we use $B = 200$ bootstrap iterations to construct PPI confidence intervals.)

Similar to Section 4, the GT-only confidence interval stays constant regardless of the bias level, and it is wider than the PPI and map-only intervals due to the small number of ground truth points ($n = 500$).

At all bias levels across all three experiments (error in X_{pop} , Y , or both), the PPI confidence intervals contain the true coefficients for both covariates. This is expected, as PPI uses the small set of ground truth points to correct for bias in the map product, and the PPI confidence intervals are guaranteed to contain the true coefficient with 95% probability.

At all bias levels, the PPI confidence intervals are significantly smaller than the GT-only intervals. This is because the biased map is a simple linear transformation of the true variable values and thus provides useful information for estimating the regression coefficients. As discussed in Section 4, PPI allows us to conclude that there is a positive association between forest cover and population, while the GT-only interval for β_{pop} contains zero and does not detect this significant association.

In all three experiments, as map bias increases, the map-only estimates become biased for at least one of the coefficients. The map-only confidence intervals are very narrow because the number of map product points is large ($N = 67968$), so they fail to contain the true coefficients as the estimates become biased. As mean reversion bias in X_{pop} increases, the map underestimates high population values and overestimates low population values. As a result, the map-only estimates for β_{pop} increase in magnitude and overestimate the true coefficient, while map-only estimates for $\beta_{\text{elevation}}$ remain unbiased (since we do not add bias to the elevation map). As mean reversion bias in Y (forest cover) increases, the map underestimates high forest cover values and overestimates low forest cover values. As a result, the map-only coefficient estimates for both covariates decrease in magnitude and attenuate toward zero. When there is mean reversion at level c in both forest cover and population, the effects of the two biases cancel out to produce unbiased map-only estimates of β_{pop} . However, the map-only estimates of $\beta_{\text{elevation}}$ still decrease in magnitude and attenuate toward zero.

Simulating the Role of Map Mean Reversion Bias

Regression specification

$$Y = \beta_0 + \beta_{\text{elevation}} X_{\text{elevation}} + \beta_{\text{population}} X_{\text{population}} + \varepsilon$$

Varying simulated bias

$$X_{\text{pop}}^{\text{map}} = c\mu_{X_{\text{pop}}} + (1 - c)X_{\text{pop}}$$

$$Y^{\text{map}} = c\mu_Y + (1 - c)Y$$

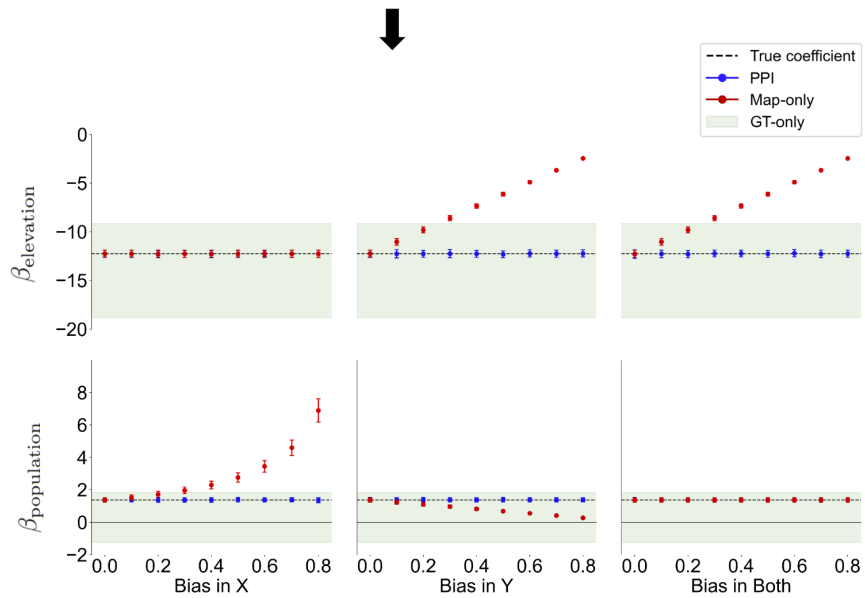


Figure 14: **Simulation estimating forest cover linear regression coefficient 95% confidence intervals under different levels of map mean reversion bias.** PPI gives unbiased estimates with much narrower confidence intervals than the GT-only method. In each experiment, the map-only coefficient estimate for at least one covariate becomes increasingly biased as map bias increases.